Wind 2015 Senior Review Proposal

Adam Szabo
NASA GSFC
Project Scientist/Presenter

Lynn B. Wilson III
NASA GSFC
Deputy Project Scientist

Executive Summary

NASA launched the *Wind* spacecraft in November, 1994 to the Earth's L1 Lagrange point as the interplanetary component of the Global Geospace Science (GGS) Program within the International Solar Terrestrial Physics (ISTP) program. The spin stabilized spacecraft – spin axis aligned with ecliptic south – carries eight instrument suites that provide comprehensive measurements of thermal to solar energetic particles, quasi-static fields to high frequency radio waves, and γ-rays. All instrument suites continue to provide valuable scientific observations completely available to the public (except the TGRS γ-ray instrument, now without coolant).

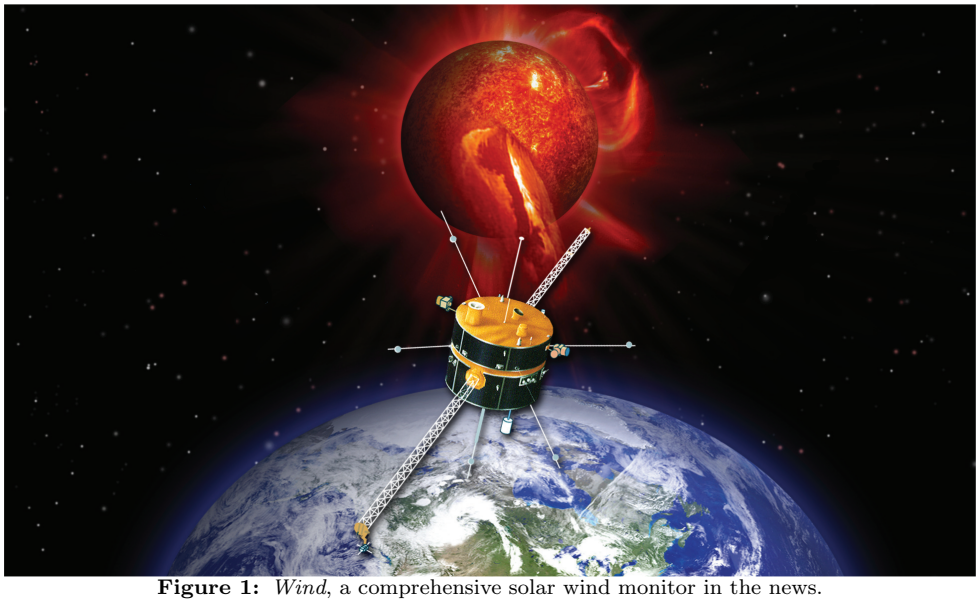

Figure 1: *Wind*, a comprehensive solar wind monitor in the news.

The *Wind* instrument suite provides comprehensive and unique high time resolution in-situ solar wind measurements that enable the investigation of wave-particle interactions. *Wind* is the only near-Earth spacecraft equipped with radio waves instrumentation. *Wind* has made numerous independent discoveries since the last Senior Review, from constraining theories of solar wind heating to direct observations of wave-driven particle acceleration and heating (see insets in Figure 1). *Wind* data have been critical to a wide range of studies resulting in **>500 refereed publications in 2013-2015** (e.g., since the last Senior Review) and **over 3600 refereed publications since launch** (listed on the *Wind* project Web page: http://wind.nasa.gov). **Since 2013, 8 graduate students earned doctoral degrees and 14 more are currently in progress using *Wind* observations.** The new results span all three heliophysics research objectives as described in the *Science Plan for NASA's Science Mission Directorate 2007-2016*. The *Wind* science data products are publicly served directly from the instrument team sites and CDAWeb, with a single project web page containing links to and descriptions of the large number of *Wind* data products. *Wind* is also an active participant in the development of the Virtual Heliophysics Observatory (VHO) that allows for more complex queries than CDAWeb.

Even though *Wind* is >20 years old, the spacecraft is still in good health and is ready for a host of new discoveries. Because of its longevity, *Wind* observations will allow researchers to compare long-term variations in solar wind properties for solar cycles 22–24 without needing to compensate for changing instrumentation and calibration. Furthermore, new *Wind* data, recalibrated this past year and already resulting in new discoveries, will **provide unprecedentedly accurate and high time, energy, and angular resolution measurements of the near-Earth 1 AU solar wind.**

Wind continues to remain a relevant mission as evidenced by recent press releases on the NASA website at:

http://www.nasa.gov/content/goddard/solar-wind-workhorse-marks-20-years-of-science-discoveries/, and
http://www.nasa.gov/content/goddard/more-than-meets-the-eye-nasa-scientists-listen-to-data/index.html

Wind has also contributed critically to multi-mission studies, as part of the Heliophysics System Observatory (HSO). With its ample fuel reserves, sufficient for ∼53 years, *Wind* will continue to provide accurate solar wind input for magnetospheric studies (supporting MMS, THEMIS, and *Van Allen Probes*) and serve as the 1 AU reference point for outer heliospheric (e.g., *Voyager*) investigations, in addition to providing critical support for other NASA missions (e.g., STEREO, ACE, etc.). Moreover, new *Wind* results will continue to improve theories of solar wind heating, acceleration, and energetic particle processes to focus the science objectives of future missions (e.g., *Solar Probe Plus* and *Solar Orbiter*). Once these new missions are launched, ***Wind* will provide critical measurements to complement the observations made by *Solar Probe Plus* and *Solar Orbiter* which will enable researchers to relate the solar wind at 1 AU to its coronal source and compare radio burst power with source locations.**

Rationale for Continuing the *Wind* Mission

- *Wind* continues to provide unique, robust, and high resolution solar wind measurements
- *Wind* will serve as the 1 AU reference for *Solar Probe Plus* and *Solar Orbiter*
- *Wind* will aid in cross-calibration efforts for the DSCOVR mission
- *Wind* and ACE together can provide 24/7 near-Earth L1 monitoring for the next >10 years
- *Wind* and ACE are complementary not identical ⇒ both are needed for complete 1 AU observations
- *Wind* still has redundant systems, instruments, and enough fuel for ∼53 years
- *Wind*'s scientific productivity remains high → significant discoveries in all three SMD research objectives

Table of Contents

1 Science and Implementation

1.1 Historical Background

The *Wind* spacecraft was launched in November, 1994 as the interplanetary component of the Global Geospace Science (GGS) Program within ISTP. *Wind*'s original purpose was (1) to make accurate in-situ measurements of interplanetary conditions upstream of the magnetosphere to complement measurements made in the magnetosphere by *Polar* and *Geotail* and (2) to remotely sense interplanetary disturbances for possible future predictive purposes. The instruments were therefore designed to make highly accurate solar wind measurements.

After a number of years at the L1 Lagrange point, *Wind* performed a series of orbital maneuvers to take it to various scientifically valuable observational points. In 1999, *Wind* executed a number of magnetospheric petal orbits that took it to the rarely sampled geomagnetic high latitudes. Between 2000 and 2002, *Wind* moved further and further away from the Sun-earth line (and ACE) reaching 350 R_E in the east-west direction in a distant prograde orbit. Finally, in 2003, it completed an L2 campaign taking the spacecraft more than 250 R_E downstream of Earth and ∼500 R_E downstream of ACE to investigate solar wind evolution and magnetotail phenomena. Since 2004, *Wind* has remained at L1 where it will stay for the foreseeable future.

1.2 Current Status

The *Wind* spacecraft continues to operate in good health. In 2000, the team successfully reconfigured the communications system to enhance the telemetry margin. Reliance on a single digital tape recorder since 1997 has never hampered operations, and the team took measures to minimize its use in order to extend tape recorder life as long as possible.

Seven of the eight *Wind* instruments, including all of the particles and fields instruments, remain largely or fully operational. The EPACT, high energy particle, and SMS solar wind composition instruments suffered some degradation, but both continue to provide valuable measurements. The SWE electron instrument required some reconfiguration to maintain its capabilities and the TGRS γ-ray detector has been turned off, as planned due to it no longer having sufficient coolant to operate. For technical details see Section 5.2.

In May 2014 the 3DP instrument (specifically PESA Low) suffered an anomaly that only affected the telemetry house keeping data. The science data remained unaffected and continues to return the highest resolution velocity moments of the solar wind of any near-Earth spacecraft. All the other instruments operate nominally. Thus, the net loss in capability remains minimal and the *Wind* instruments continue to provide definitive and continuous measurements of the solar wind.

On Oct. 27, 2014 at 21:59:38 GMT, the *Wind* command and attitude processor (CAP) suffered two single event upsets (SEUs). The redundant nature of the *Wind* spacecraft bus allowed the flight operations team (FOT) to successfully switch to a second CAP. The FOT began the recovery of CAP1 on Jan. 21, 2015 and finished Jan. 30, 2015. Thus, the *Wind* spacecraft was fully recovered at ∼17:50 UTC on Jan. 30, 2015. For more details, please see Section 5.2.

In conclusion, *Wind* is operationally healthy and continues to maintain a large fuel reserve, capable of sustaining the spacecraft at L1 for almost ∼53 years.

1.3 *Wind*'s Unique Capabilities

Wind's complement of instruments was optimized for studies of solar wind plasma, interplanetary magnetic field, radio and plasma waves, and of low energetic particles. The instrument suite is not equivalent to that on ACE; rather the two missions complement each other. ACE – launched a few years after *Wind* – focuses on the detailed investigation of high energy particles for which *Wind* has limited capabilities. Several of the *Wind* solar wind, suprathermal particle, and especially radio and plasma wave instruments are unique. *Wind*'s instrument capabilities are summarized in Table 1 and are compared to ACE and STEREO. ***Wind* is unparalleled for low energy particle and radio wave observations of the solar wind by near-Earth spacecraft.** A more detailed discussion of the unique *Wind* capabilities follows in the next paragraphs.

Collaborating with STEREO, *Wind*/WAVES provides an essential third vantage point along the Sun-Earth line, allowing the unambiguous localization of inner heliospheric radio sources and the determination of their corresponding beam patterns. In case STEREO B cannot be recovered, *Wind* will be able to replace the STEREO B plasma, magnetic field, and electromagnetic waves measurements still allowing STEREO A/*Wind* two-point observations. More importantly, *Wind* is the only spacecraft at L1 that can observe the thermal noise regime of the plasma, which provides the most accurate measurement of the local electron plasma frequency in the solar wind. This quantity is directly proportional to the square root of the electron number density. Thus, the density – normally obtained as a moment or fit of the velocity distribution function from particle instruments like SWE and 3DP – can be accurately and independently derived from the WAVES instrument. The WAVES instrument provides the only method for an independent, in-flight, and absolute calibration for particle instruments for spacecraft near L1.

Wind is unparalleled in its capacity for high time resolution (HTR) measurements of quasi-static magnetic fields (MFI instrument) and thermal solar wind elec-

Table 1: The measurement capabilities of *Wind* compared to STEREO and ACE

Type	*Wind*	STEREO	ACE	Comments for *Wind*
DC Magnetic Field	MFI ∼11 sps[a]	MAG ∼8 sps, (∼32 sps burst)	MAG ∼6 sps	highest time resolution for continuous coverage
Radio Waves	WAVES ∼4kHz–14MHz	S/WAVES ∼2.5kHz–16MHz	N/A	unique large antenna length allows for measurement of local plasma frequency → electron density
Time Domain Waveforms	TDS ∼1.9–120ksps[b]	TDS ∼7.8–250ksps	N/A	search coil and long antenna → better calibration and more sensitive
Thermal Ions (Moments)	3DP[c] SWE ∼92 s	PLASTIC ∼60 s	SWEPAM ∼64 s	highest time, angular, and energy resolution; robust and redundant; operates during solar storms
Thermal Ions (DFs[d])	3DP ∼24 s[e]	PLASTIC N/A	SWEPAM N/A	highest time, angular, and energy resolution
Thermal Electrons (Moments)	3DP (∼3 s) SWE (∼9 s)	SWEA[f] (∼2 s)	SWEPAM (∼128 s)	highest time resolution for full 4π coverage at low energy
Thermal Electrons (DFs)	3DP ∼3 s	SWEA ∼2 s	SWEPAM N/A	[same as above]
Solar Wind Composition	SMS/STICS 1≤Z≤56 ∼0.3–230keV/Q	PLASTIC 1≤Z≤56 ∼0.3–80keV/Q	SWICS 1≤Z≤30 ∼0.5–100keV/Q	only observations > 100 keV/Q
Mass Spectrometry	SMS/MASS 1≤Z≤28 ∼0.5–12keV/Q	N/A N/A N/A	SWIMS 2≤Z≤30 ∼0.5–20keV/Q	comparable to ACE in both charge and energy
Low Energy Electrons	3DP ∼3eV–500keV	SWEA[g] SEPT[h] STE[i]	SWEPAM EPAM ∼3eV–400keV	full 3D measurements from a few eV to ∼500 keV
Low Energy Ions	3DP ∼3eV–7MeV	SEPT ∼60keV–7MeV	SWEPAM[j] EPAM[k] ULEIS[l]	measurements of solar wind thermal core to lower energies
High Energy Particles	EPACT/LEMT ∼0.04–50MeV/n	SIT[m] LET[n] HET[o]	SIS CRIS ∼10–600MeV/n	robust; high geometry factor; unique directional observations; and energy range

[a] ∼22 samples per second when inside 100 R_E; [b] kilosamples per second; [c] moments: ∼3s, distributions: ∼24s, burst: ∼3s; [d] DF = velocity distribution function; [e] ∼3s in burst mode; [f] nothing below ∼60eV; [g] ∼60–3000eV; [h] ∼2–100keV, 4/8 telescopes contaminated; [i] ∼30–400keV; [j] ∼260eV–35keV; [k] ∼46–4800keV; [l] ∼45keV/n–2MeV/n; [m] ∼0.03–5MeV/n; [n] ∼2–60MeV/n; [o] ∼1–170MeV/n;

trons (3DP). Though STEREO/SWEA has a higher cadence in burst mode, the low energy (≲60 eV) electrons are contaminated, causing *Wind*/3DP to have the highest time resolution measurements of thermal electrons. *Wind*/MFI offers continuous coverage of the quasi-static magnetic fields at ∼11 samples per second (sps) over the entire mission (∼22 sps when *Wind* was within ≲100 R_E of Earth), still the highest sample rate of continuous solar wind measurements.

Wind/STICS is unique among currently operational spacecraft as it is the only sensor in space fully dedicated to providing measurements of heavy ions for an energy range spanning ∼6.2–223.1 keV/amu. As STICS is a time-of-flight mass spectrometer, it can differentiate many minor ionic species and look at their characteristics in the suprathermal energy range to better understand their origin. In addition, *Wind*/LEMT provides high energy particle data over a range of energies not covered by ACE.

The *Wind*/WAVES instrument can also be used for solar energetic particle (SEP) studies. For instance, *Malandraki et al.* [2012] and *Agueda et al.* [2014] made detailed comparisons of the injection time histories of selected SEP events, as derived from the modeling

of the interplanetary transport of electrons and protons, with electromagnetic emissions, particularly with decametric-hectometric (DH) type III radio bursts. A close correspondence was found, and this underlines the usefulness of type III bursts as a constraint of energetic particle release to interplanetary space. *Wind* is still the only near-Earth spacecraft which can measure both the electromagnetic and particle signatures of SEP events. **Thus, *Wind*'s distinct capacities make it as a valuable asset to the Heliophysics community and an essential component in the HSO.**

1.4 Heliophysics System Observatory

Wind plays an active role in the Heliophysics System Observatory (HSO). *Wind* achieved many of its recent scientific discoveries in collaboration with other spacecraft as described in more detail in Section 4. However, the HSO is more than just the occasional comparison of data from multiple platforms. It is a data environment where such comparisons can be readily performed. As the Heliophysics Data Policy outlines, this data environment requires the presence of in-depth metadata for each data product based on a uniform standard (the SPASE dictionary). It also envisions the eventual connection of the distributed data repositories by a number of virtual observatories enabling the location and downloading of the desired data. *Wind* plays a leadership role in the deployment of the Virtual Heliospheric Observatory (VHO), the heliospheric portion of this environment, and the generation of the corresponding metadata.

The Living With a Star (LWS) program seeks to better understand the Sun-Earth connected system with the aim of developing reliable space weather forecasting capabilities. The program architecture plan calls for a near-Earth solar wind monitor to connect the solar (SDO) and inner heliospheric (*Solar Probe Plus* and *Solar Orbiter*) observations with geomagnetic ones (MMS). However, NASA has no current plans for a new solar wind monitoring mission. Rather NASA assumes that *Wind*, ACE or both will survive into the 2015–2022 time frame. DSCOVR has only limited measurement capabilities (Faraday Cup and magnetometer) and fuel only for about five years, leaving *Wind* and ACE still as the primary near-Earth assets during the primary phase of the *Solar Probe Plus* and *Solar Orbiter* missions. The lowest risk option to satisfy the near-Earth solar wind monitoring requirement of LWS is to sustain both *Wind* and ACE – either of which can satisfy the LWS measurement requirements – because both are well past their prime missions and design lifetimes. Again, note that *Wind* and ACE are not duplicate spacecraft but rather serve complementary roles. Thus, the most prudent course of action involves preserving both spacecraft.

2 Old Prioritized Science Goals

Old Prioritized Science Goals

1. Long-term Variation Covering 2 Solar Cycles
   (a) Solar Wind Abundance Variations
   (b) SEP variations
2. Acceleration and Heating of the Solar Wind
3. The Propagation and Evolution of ICMEs
   (a) Local and Global Distortions of ICME Geometry
   (b) Why do some CMEs evolve into irregular ejecta?
4. Dust science

The *Wind* mission is operating on a minimal budget that does not allow for the dedicated support of any in-depth focused scientific research. The funding is applied to the operation of the spacecraft and the collection and validation of high quality solar wind measurements. While, as part of the instrument data validation process, quite a number of significant scientific discoveries have been made even in recent years as outlined in the previous sections, most detailed scientific research using *Wind* data is primarily supported under ROSES GI and SR&T. In the following sections, we outline a number of *Wind* results relating to our past focused science research topics.

2.1 PSG#1: Solar Cycle Variations

The most recent solar minimum was unusually prolonged and the following solar maximum abnormally small. The long-term, 20-year solar wind observations of the *Wind* spacecraft enabled the comparison of solar wind conditions over multiple solar cycles. *McComas et al.* [2013], using primarily *Wind* and IMP 8 data, have found the that the solar wind density, velocity and temperature decreased significantly during the most recent solar cycle and that this decrease is concurrent with a magnetic field magnitude and radial component reduction. They argue that there is a causal connection between the reduced solar magnetic flux and solar wind power. The reduced solar wind pressure has implications to the size of planetary magnetospheres and the location of the heliopause quite likely leading to the Voyager spacecraft traveling into interstellar space.

Another consequence of the current diminished solar cycle is extremely mild space weather conditions. *Gopalswamy et al.* [2014] reported that the number of major geomagnetic storms and high-energy solar energetic particle events are at the lowest since the dawn of the space age. *Gopalswamy et al.* [2014] explained the mild space weather as a consequence of the anomalous expansion of CMEs, relative to previous solar cycles, and the weak state of the heliosphere. The anomalous expansion results in the dilution of the magnetic contents of CMEs, so the geomagnetic storms are gen-

erally weak. CME-driven shocks propagating through the weak heliospheric field are less efficient in accelerating energetic particles, so the particles do not attain high energies.

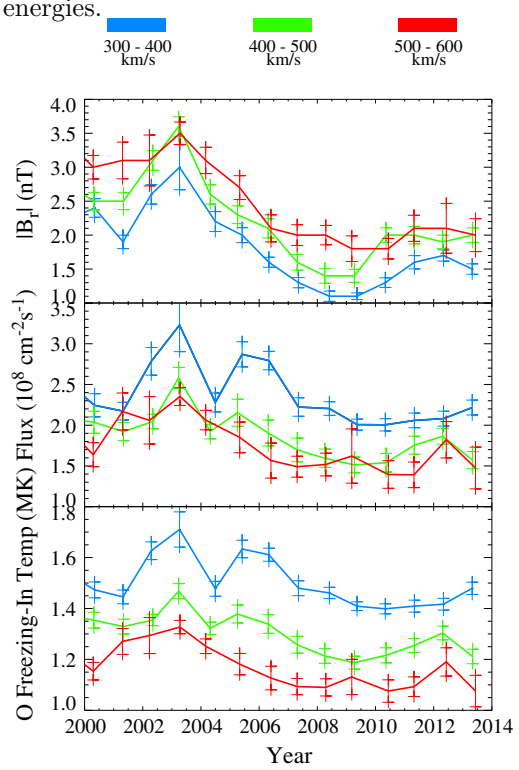

Figure 2: The figure shows long-term variations in color-coded speed bins and in 0.75 year time-bins. The figure panels are: (top) the unsigned radial magnetic field strength, which serves as a proxy for the magnetic flux in solar wind; (middle) OMNI data 1 AU particle flux, bin by speed and form 1 year medians and uncertainties; and (bottom) coronal freezing-in temperature deduced from O^{7+}/O^{6+} charge state ratio. Figure adapted from *Schwadron et al.* [2014].

However, *Richardson et al.* [2014] identifying over 200 >25 MeV proton events observed at the STEREO spacecraft and near Earth in 2006-2013, extending from the minimum preceding cycle 24 to the peak of the cycle, found no significant reduction in the number of these energetic events during the current solar maximum. They have used *Wind*/WAVES observations of type II and type III bursts to help identify the solar sources of each event to resolve this puzzle.

Cliver et al. [2013] used a decomposition of the solar wind into CMEs, high speed streams, and slow solar wind based on *Wind* and ACE data to show that solar wind B variation is transmitted to the heliosphere primarily via CMEs at solar maximum and high speed streams from polar coronal holes at solar minimum. Thus the weak solar polar fields at the solar minimum between cycles 23 and 24 [**?**] resulted in record high cosmic ray intensities in 2009. A comparison of average solar wind B and the tilt angle of the heliospheric current sheet for this year challenged the conventional view that particle drift rather than diffusion dominates cosmic ray modulation at solar minimum.

2.1.1 Solar Wind Abundance Variations

The solar wind scaling law relates a solar wind stream's 1 AU speed to coronal electron temperature and to particle flux near its source. The solar wind scaling law follows from scaling injected Poynting flux and particle flux based on large-scale magnetic flux in the heliosphere. The scaling law takes into account energy losses in the form of heat conduction and gravitational potential. Thus, this model can predict changes in the corona based upon the evolution of the heliospheric magnetic field.

Schwadron et al. [2014] found not only the increase in coronal temperatures of cycle 24 but also a drop of coronal temperatures in the most recent data. Figure 2 shows extended analysis of the scaling law into cycle 24 using OMNI data (which relies heavily upon ACE and *Wind*). This result suggests not only that we may have already extended through the cycle 24 maximum in 2013, but also that we have begun descent into the cycles 24-25 minimum for the 400-500 and 500-600 km/s speed bins. Coronal temperatures continue to show remarkably low values indicative of the anomalous lack of solar activity in the era that began approximately in 2005.

Schwadron et al. [2014] found that the reductions in sunspot number appear to be associated with lower freezing-in temperature in 2013. The reduction in coronal electron temperature in the cycles 23-24 protracted solar minimum is similar to reductions observed at the beginning of the Dalton Minimum (∼1805-1840). If these trends continue to reflect the evolution of the Dalton Minimum, we will observe further reductions in coronal temperature in the cycles 24-25 solar minimum.

2.1.2 Solar Activity Variation

In a recent series of articles in the Astrophysical Journal, McIntosh and collegues argued for the hypothesis that elements of the sunspot cycle and solar activity can be explained as a consequence of the intra- and extra-hemispheric interaction between overlapping activiy bands of the sun's 22-year magnetic polarity cycle. In an article recently accepted for publication in Nature Communications, a self-consistent extension of the theory into teh coronal and heliospheric domain was presented [*McIntosh et al.*, 2015]. McIntosh and colleagues demonstrated that the quasi-annual variability of coronal magnetism predicted by the theory is evident in strong signatures in the solar wind speed and helium abundance over the last three solar cycles. The solar wind helium abundance – a proxy for plasma heating at the point of origin – was shown to reflect both the long-term weakening of the solar dynamo and the quasi-periodic variability driven by magnetic surges from the

activity bands.

The activity band interaction theory constitutes a novel and powerful new paradigm, in particular for forecasting solar activity over timescales of years to decades. The multi-cycle record of solar wind hydrogen and helium provided by *Wind* and its OMNI extensions enabled the investigators to explore and distinguish between secular and short-term signatures consistent with the theory. This was a critical compliment to the multi-cyclical sunspot, irradiance, and magnetographic records that formed the backbone of the study.

2.1.3 SEP Variation

The LEMT telescope, part of the *Wind*/EPACT instrument suite, was designed to measure the abundances of elements in energetic particles and to extend those measurements to elements throughout the periodic table. The element abundances in the large gradual solar energetic-particle (SEP) events are swept up from the corona and accelerated by shock waves driven out from the Sun by CMEs. Their abundances, like those of the corona and solar wind, differ from photospheric abundances by a factor which depends upon the first ionization potential (FIP) of the element, low (<10 eV) FIP elements being enhanced by a factor of about 4 from those with high FIP [*Reames*, 2013, 2014].

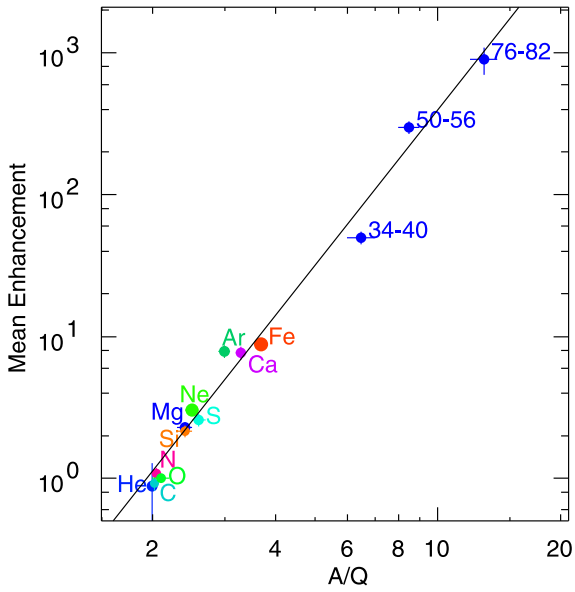

Figure 3: The power-law dependence of the mean enhancement of element abundances in impulsive SEP events relative to coronal abundances is shown vs. A/Q. The strong power-law dependence allows us to determine the pattern of Q and, hence, the source plasma temperature. Figure adapted from *Reames et al.* [2014a].

In contrast, the elements in impulsive SEP events, associated with solar flares and jets, have relative abundances that increase strongly throughout the periodic table, from an average factor of ∼3 at Ne, to ∼9 at Fe to ∼900 for $76 \leq Z \leq 82$ [*Reames et al.*, 2014b]. This strong increase in element abundances, relative to coronal abundances, actually has a power-law dependence upon the mass-to-charge ratio, A/Q of the element as seen in Figure 3. This strong power-law dependence on A/Q is understood to be a consequence of magnetic reconnection on open field lines along which the SEPs escape. Since the enhancements depend upon A/Q, and Q depends upon the plasma temperature, we can use the observations in each impulsive SEP event to determine the source plasma temperature of the acceleration site [*Reames et al.*, 2014a]. This temperature of 2-4 MK (million degrees Kelvin) is typical of a solar active region, but is much lower than the >10 MK seen in solar flares. However, the hot regions in solar flares tend to occur on closed loops, which contain the energy of reconnection, while nearby open field would allow the accelerated ions and electrons to escape along with any CME plasma ejected.

2.2 PSG#2: Solar Wind Kinetic Physics

Pulupa et al. [2014] examined electron heating in magnetic reconnection exhausts in the solar wind. Figure 4 shows heating of the core electron population within a solar wind reconnection exhaust. The *Wind*/WAVES thermal noise spectrum (panel (a)) enables very accurate detection of the electron density in the plasma. Using this density as a reference, the spacecraft potential can be calculated and used to correct the electron measurements from *Wind*/3DP. These corrected measurements, in turn, enable sensitive measurements of small changes in the core electron temperature, such as the several eV heating observed in the reconnection exhaust shown. These results, which were enabled by the complementary fields and particle instruments onboard *Wind*, are the first measurements of electron core heating in solar wind reconnection exhausts.

Kasper et al. [2008] statistically analyzed measurements from *Wind*'s Faraday cup to explore α-to-proton temperature ratio: $\theta_{\alpha p} \equiv T_\alpha / T_p$. The probability distribution of $\theta_{\alpha p}$ values is plotted with a green, dashed curve in Figure 5 and has two, particularly noteworthy features. First, consistent with observations from other spacecraft [*Hefti et al.*, 1998; *Marsch et al.*, 1982a; *Schmidt et al.*, 1980; *von Steiger et al.*, 1995], α–particles are almost always hotter than protons. Indeed, $\theta_{\alpha p} < 1$ occurs in only 1.1% of the dataset used in Figure 5. Second, the $\theta_{\alpha p}$–distribution is strongly bimodal. The lower mode ($\theta_{\alpha p} = 1.2$) indicates near thermal-equilibrium, and the higher mode ($\theta_{\alpha p} = 4.5$) roughly corresponds to mass proportional temperatures. These two modes are predominately associated with slow and fast wind, respectively. Nevertheless, the qualitative analysis of *Kasper et al.* [2008] suggested that $\theta_{\alpha p}$ is more correlated with collisional age [an es-

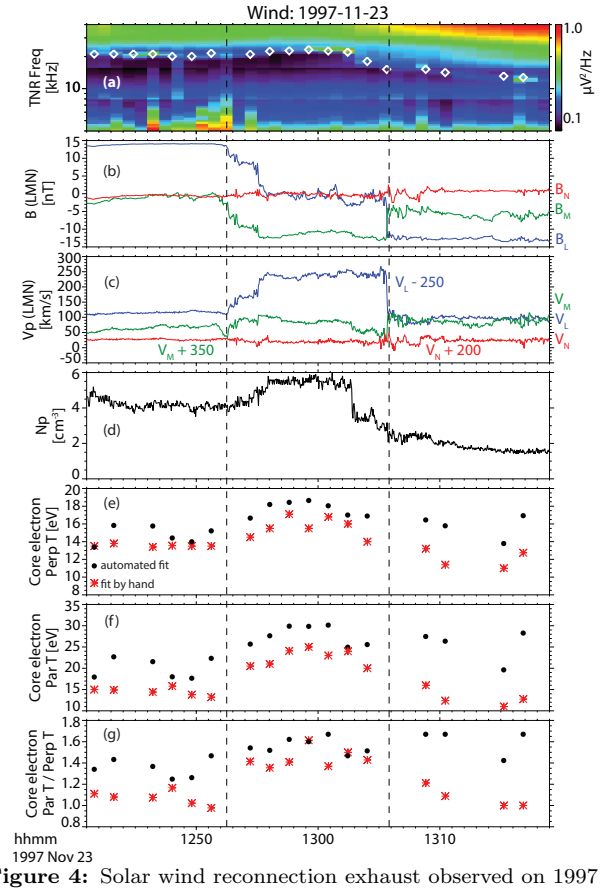

Figure 4: Solar wind reconnection exhaust observed on 1997 November 23. Panel (a) shows the thermal noise spectrum from the *Wind*/WAVES TNR, with the electron densities derived from the plasma line shown as white diamonds. Panel (b) shows the magnetic field observed at *Wind* in *LMN* minimum variance coordinates. Panel (c) shows the proton *LMN* velocity, while panel (d) shows the proton density. The core electron perpendicular temperature is shown in panel (e), the core parallel temperature in panel (f), and the ratio of parallel to perpendicular core temperature in panel (g). Temperatures derived from automated fitting techniques are shown as black dots; temperatures derived from hand optimization of the fitting technique are indicated by red asterisks. Dashed vertical lines denote the boundaries of the exhaust. Figure adapted from *Pulupa et al.* [2014].

timate of the degree to which plasma has thermalized in going from the Sun to the spacecraft; see *Feldman et al.*, 1974; *Neugebauer*, 1976] than with solar-wind speed.

Maruca et al. [2013] significantly extended the analysis of *Kasper et al.* [2008] by developing an analytic model for the collisional thermalization of protons and α–particles [*Huba*, 2011]. Empirical radial trends in ion density, speed, and temperature [*Hellinger et al.*, 2011] were incorporated in this model so that a $\theta_{\alpha p}$–value measured in a parcel of plasma at a given distance from the Sun could be used to infer that parcel's $\theta_{\alpha p}$–value at some other distance. *Maruca et al.* [2013] performed such an analysis for 2.1–million $\theta_{\alpha p}$–values measured at 1.0 AU with the *Wind* Faraday cups and estimated

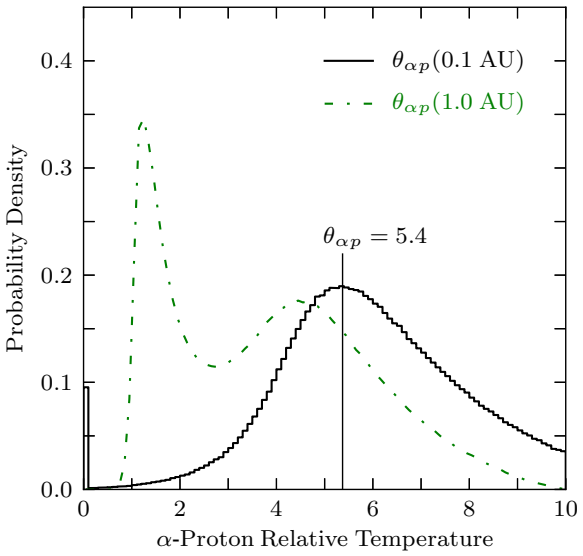

Figure 5: From *Maruca et al.* [2013], probability distributions of values of α-proton relative temperature: $\theta_{\alpha p} \equiv T_\alpha/T_p$. The green, dashed curve shows the distribution of 2.1-million $\theta_{\alpha p}$-values observed at 1.0 AU from the Sun with the *Wind* spacecraft. The black, solid histogram shows the distribution of corresponding $\theta_{\alpha p}$-values at 0.1 AU as inferred from an analytic model of collisional thermalization. While the former distribution is strongly bimodal, the latter is monomodal. This suggests that the corona preferentially heats α-particles to similar degrees for both the slow and fast wind.

the corresponding $\theta_{\alpha p}$–values at 0.1 AU (i.e., near the Alfvén critical-point). The probability distribution of these inferred $\theta_{\alpha p}$(0.1 AU)–values is plotted as a black, solid histogram in Figure 5. Remarkably, this distribution is monomodal even though the distribution of observed $\theta_{\alpha p}$(1.0 AU)–values is bimodal. This indicates that collisional thermalization, in and of itself, can account for this bimodality. Low $\theta_{\alpha p}$–values are predominantly associated with slow wind, and high $\theta_{\alpha p}$–values with fast wind. Nevertheless, this correlation does not seem to arise from slow and fast wind having different coronal heating profiles but simply from slow wind having a longer expansion time and typically higher rates of ion collisions.

One long standing question in solar wind turbulence is what physical processes cause the steepening of the power spectrum of magnetic fluctuations at ion kinetic scales. One way to approach this question is to measure the spatial scale which the steepening corresponds to, since different scales are associated with different processes. Previously, the problem with this approach was that in the solar wind at 1 AU two of the primary theoretical scales, the ion gyroradius and the ion inertial length, typically take the same value because $\beta_i \sim 1$. *Chen et al.* [2014] took advantage of the large *Wind* data set to find the rare periods when β_i was much larger or smaller than 1 so that these scales could be successfully distinguished. As shown in Figure 6, it was

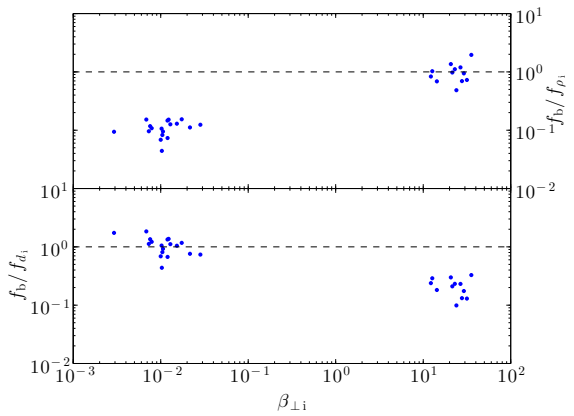

Figure 6: Ratio of measured spectral break frequency to the frequency corresponding to the ion gyroradius (upper panel) and ion inertial length (lower panel) as a function of perpendicular ion plasma beta. For low beta the break matches the ion inertial length and high beta the ion gyroradius. Figure adapted from *Chen et al.* [2014].

found that the break happens at which ever of the two scales is larger under the given conditions, and the implications of this result are actively being debated by the solar wind turbulence community. They are important for our understanding of kinetic turbulence and how it heats the solar wind [*Chen et al.*, 2014]. This result was only possible due to the high resolution instrumentation on *Wind*, together with the long data set, which enabled the necessary rare solar wind conditions to be sampled.

In a study of a reconnection layer at high northern latitudes observed by the *Polar* spacecraft, *Muzamil et al.* [2014] used *Wind* as an upstream monitor. *Wind* observed an interplanetary field of 20 nT which pointed strongly northward continuously for 13 hr (see Figure 7). So when *Polar* observations started, reconnection had already been ongoing for several hours. This was confirmed by DMSP F13 passes which documented reverse polar cap convection for many hours, thus providing direct evidence of continued reconnection. *Polar* observed sunward and southward jets. The event was hallmarked by a density asymmetry ≈140 and moderate guide field. Thus, a reconnection layer can be studied under extreme asymmetric conditions.

This is, to our knowledge, the first study of a high-latitude reconnection layer with (1) an extreme density asymmetry and (2) steady and continuously strong interplanetary B_z. **Such an investigation is a kind of forerunner of what can be done by combining interplanetary (e.g., *Wind*) and in-situ data at reconnection sites when MMS is launched.**

Wind observed a boundary layer tailward of the dawn terminator which is entirely populated by rolled-up flow vortices on Oct. 24, 2001 near X ∼ -13 R_E (see Figure 8). The results were reported by *Farrugia et al.*

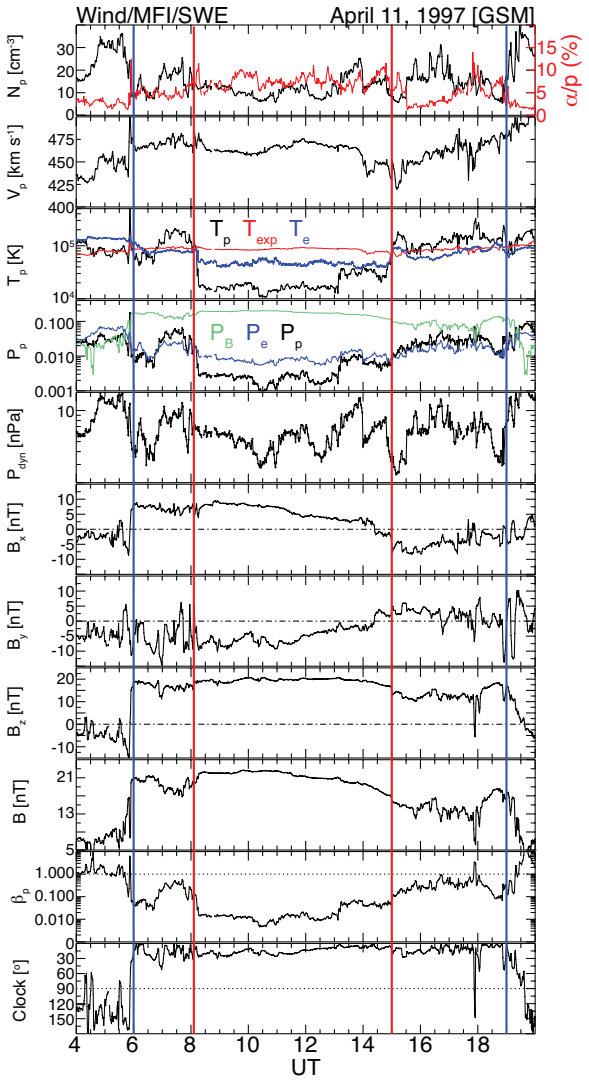

Figure 7: *Wind*/SWE and MFI observations during 420 UT, 11 April 1997. The panels display the proton density (in red the α-to-proton number density ratio in % with scale on the right), bulk speed, temperatures (proton temperature in black, electron temperature in blue, and the expected proton temperature in red), pressures (proton pressure in black, electron pressure in blue, and the magnetic pressure in green), dynamic pressure, the components of the magnetic field in GSM coordinates, total field strength, proton β, and the IMF clock angle. The blue vertical lines show the estimates of the interplanetary coronal mass ejection (ICME) boundaries, 6–19 UT. Between the red lines is our identification of the MC embedded in the ICME. Figure adapted from *Muzamil et al.* [2014].

[2014]. Interplanetary conditions were steady with a near-radial interplanetary magnetic field (IMF). Approximately 15 vortices were observed over the 1.5 hour duration of *Wind*'s crossing, each lasting 5 min. That these vortices were rolled up was inferred from the presence of a hot tenuous plasma being accelerated to speeds higher than in the adjoining magnetosheath, a circumstance which has been shown to be a reliable signature of this in single-spacecraft observations.

A blob of cold dense plasma was entrained in each

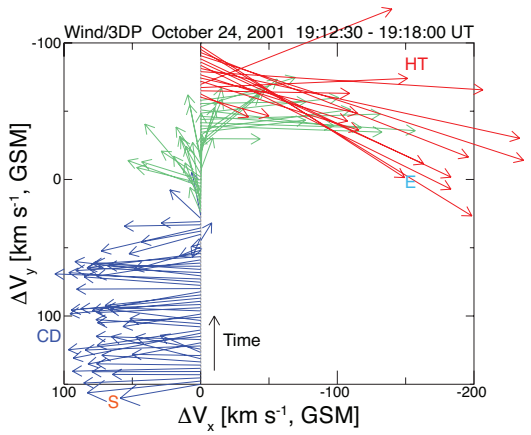

Figure 8: Residual vectors in the XY plane for one of the repetitive flow structures seen by *Wind*. Symbols S and E mark the start and end of the structure. The labels CD and HT refer to "cold dense" and "hot tenuous," respectively. Time runs from bottom to top. The blue, green, and red vectors represent differing plasma parameters. In the average velocity frame shown, the flows start moving sunward and slightly duskward (blue). They then rotate dawnward and become progressively antisunward (green) and finish flowing antisunward and duskward (red). Figure adapted from *Farrugia et al.* [2014].

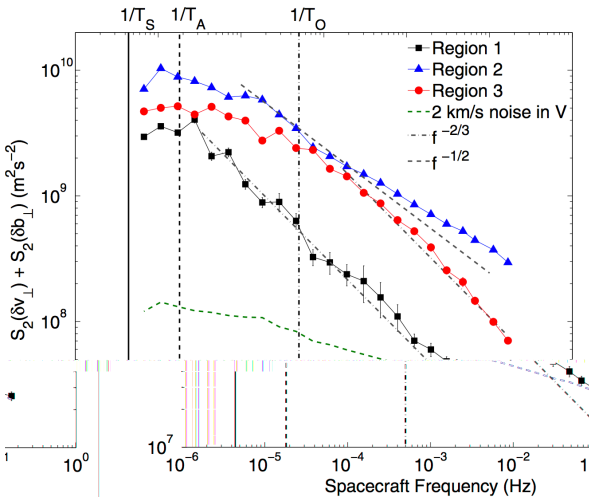

Figure 9: Sum of the velocity and magnetic-field structure functions in three regions of the σ_c, σ_r plane: Region 1, which contains balanced, equipartitioned fluctuations; Region 2, which contains very pure anti-Sunward Alfvénic fluctuations; and Region 3, which contains very pure magnetic fluctuations. Figure adapted from *Wicks et al.* [2013].

vortex, at whose leading edge abrupt polarity changes of field and velocity components at current sheets were regularly observed. In the frame of the average boundary layer velocity, the dense blobs were moving predominantly sunward and their scale size along X was X ~ 7.4 R_E. *Farrugia et al.* [2014] analyzed the stability of the boundary layer to sheared flows using compressible magnetohydrodynamic Kelvin-Helmholtz theory with continuous profiles for the physical quantities. They used parameters from (i) the exact theory of magnetosheath flow under aligned solar wind field and flow vectors near the terminator and (ii) the *Wind* data. It was shown that the configuration was indeed Kelvin-Helmholtz (KH) unstable. **This is the first reported example of KH-unstable waves at the magnetopause under a radial IMF.**

Wicks et al. [2013] used the *Wind* spacecraft MFI and 3DP instrument measurements of magnetic field vector, proton density and velocity to measure to effect of the geometrical alignment and amplitude of turbulent fluctuations on the onset frequency and power law scaling of the turbulent cascade in a single fast wind stream. They separated the times when velocity and Alfvénic magnetic fluctuations are aligned (region 2), when magnetic fluctuations dominate over velocity (region 3), and when the two are equal in magnitude but are orthogonal to one another (region 1). These regions are measured locally and in a scale dependent way and so do not correspond to average stream properties, as all previous studies have used, but instead represent the characteristics of the local fluctuations. The Region 1 structure functions (fluctuations) scale steeply from a low frequency, indicating that they readily become turbulent, but the Region 2 and 3 fluctuations maintain a flat structure function scaling to a much higher frequency, indicating that it requires more interactions or larger amplitudes to force fluctuations with these properties to become turbulent. This matches very well with theoretical predictions for the behavior of MHD turbulence and is a stringent test on theories of MHD turbulence.

The conclusion is that there may be a selective cascade of the most un-aligned fluctuations resulting in the high cross-helicity states of the solar wind in the inner heliosphere. This type of measurement is only possible with spacecraft that can measure both proton distributions and magnetic fields with high accuracy and high cadence (~1 Hz) because large amounts of stationary data are required. *Wind* is the only currently operating spacecraft permanently in the solar wind that is capable of making such observations.

2.3 PSG#3: ICME Evolution

The comprehensive *Wind* ICME list can be found at:
http://wind.nasa.gov/index_WI_ICME_v0.htm
and the corresponding Harvard-Smithsonian *Wind* Interplanetary Shock Database can be found at:
http://www.cfa.harvard.edu/shocks/wi_data/.

Both lists have been updated through most of 2014. The ICME list contains information about each ICME including start/end times, whether the ejecta produced a shock (i.e., the Harvard-Smithsonian link above), the type of magnetic obstacle (e.g., flux-rope), maximum magnetic field magnitude, mean solar wind bulk flow velocity in the ejecta, expansion velocity along the sun-Earth line in the ejecta, and links to data and model

fit plots.

The *Wind* Interplanetary Shock Database contains the relevant fitted shock parameters [e.g., see *Koval and Szabo*, 2008] for every IP shock identified using *Wind* observations. Both of these lists are updated and maintained by active members of the *Wind* team.

2.3.1 ICME Arrival Times at Earth

Making use of the opportunity for quadrature observations from STEREO and SOHO, *Gopalswamy et al.* [2013a] tested the capability of the empirical shock arrival (ESA) model for a set of 20 Earth-directed halo CMEs observed by SOHO at the Sun and *Wind* and/or ACE at Earth. The CME speeds near the Sun were measured using STEREO coronagraph images. It was found that the ESA model predicts shock arrival with a mean absolute error of 7.3 ± 3.2 h. The performance was comparable to that of the ENLIL model. It was demonstrated that CME-CME interaction and CME-coronal hole interaction can lead to large deviation from the ESA model.

Möstl et al. [2014] used three different methods for tracking and predicting CME propagation, for a dataset of 22 CMEs, with a single heliospheric imager (HI) instrument. The results were tested with in-situ field and plasma observations from STEREO IMPACT/PLASTIC and the *Wind* SWE and MFI instruments (e.g., see Figure 10 for example). This is the first dedicated study to test the predictions of CME properties with a HI instrument using a statistically significant dataset. The resulting predicted lead time using "SATPLOT", which combines coronagraph and HI observations from STEREO, was on average -1 ± 0.5 days. *Möstl et al.* [2014] found that speed and arrival time predictions were such that (1) the absolute difference between predicted and observed arrival times was 8.1 ± 6.3 hr (rms value of 10.9 hr), and (2) speeds were consistent to within 284 ± 288 km/s. To compensate for CME deceleration in the solar wind, they introduced empirical corrections to the predictions. These enhanced their performance for the arrival times to 6.1 ± 5.0 hr (rms value of 7.9 hr), and for the speeds to 53 ± 50 km/s.

The study also discovered a linear relationship between the ICME speed and the maximum in the measured magnetic field, an important parameter in predicting a CME's geoeffectivness. For two out of three events in their sample, the maximum magnetic field in the ICME interval could be predicted within a precision of 5 nT based solely on the ICME speed. **This opens up the future possibility to study the predictions of ICME arrival time and speed. Forecasting in-situ properties (arrival time, speed and field magnitude) of coronal mass ejections (CMEs) from remote images by a spacecraft far from Earth will advance the space weather effort.**

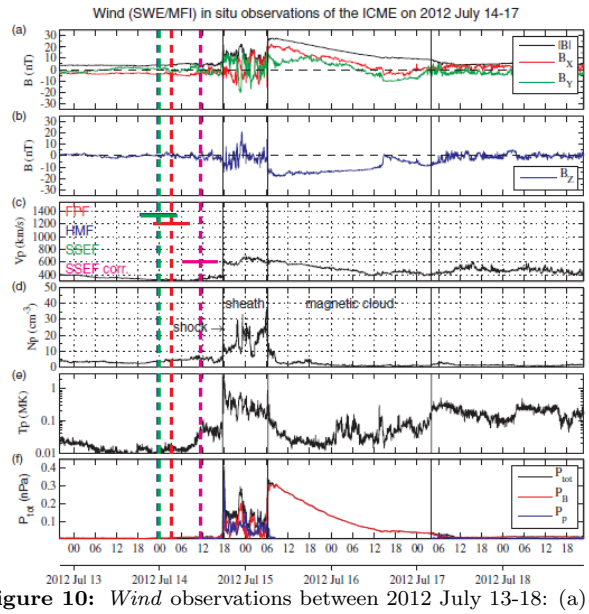

Figure 10: *Wind* observations between 2012 July 13-18: (a) total field strength and its GSE B_x and B_y components; (b) GSE B_z, (c)-(e) proton bulk speed, number density and temperature; and (f) magnetic, thermal and total pressures. The predicted arrival times from **FPF (red)**, **HMF (blue)**, and **SSEF (green)** are shown by dashed vertical lines. The speeds predicted by these models are shown in same colors by horizontal bars in panel (c) to be compared directly with the in-situ proton speed. The width of the horizontal bars corresponds to the estimated error in arrival times resulting from the manual selection of points (±10% of the total CME transit time). The corrected arrival times are shown in pink. Figure adapted from *Möstl et al.* [2014].

2.3.2 ICME Geometry Distortions

Interplanetary coronal mass ejections (ICMEs) are the main drivers of space weather. Therefore, a precise forecasting of their likely geo-effectiveness relies on accurate tracking of them. Direct white light measurements of key features of expanding ICMEs, as projected on the plane of sky, was used to extract kinematic information of these heliospheric structures by *Nieves-Chinchilla et al.* [2013]. Their main assumptions to model the ICME evolution were: radial propagation and self-similar expansion. Both assumptions imply constant ICME Position Angle (PA) and/or angular width (α) as measured by the remote-sensing observations of coronographs and heliospheric imagers. This technique allowed the identification of departure from strict radial propagation and self-similar expansion using only 2D kinematic profiles (Figure 11).

The use of different viewpoints combined with in-situ multipoint observations from NASA-ESA heliospheric observatories shows that, at least in some cases, ICMEs clearly deflected and their geometry distroted [*Nieves-Chinchilla et al.*, 2013]. The study confirmed that both overexpansion and twisting occurs as ICMEs travel toward 1 AU.

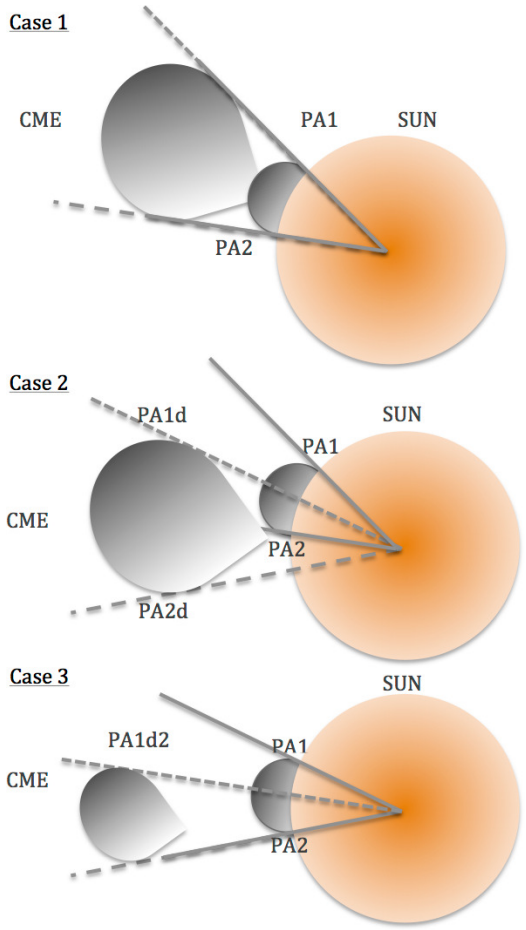

Figure 11: Three possible scenarios of ICME propagation and evolution. Case 1: radial propagation with self-similar expansion. Case 2: Deflection from radial propagation but with self-similar expansion. Case 3: Deflection with distortion of geometry. Figure adapted from *Nieves-Chinchilla et al.* [2013].

The work by *Nieves-Chinchilla et al.* [2013] showed an analysis of the morphological and kinematical evolution of a STEREO-B–directed CME on 2009 August 25-27. By means of comprehensive analysis of remote imaging observations provided by the SOHO, STEREO, and SDO missions, and in-situ measurements recorded by *Wind*, ACE, and MESSENGER, they demonstrated that the event observed near Earth was the same event as observed in-situ by STEREO-B.

Nieves-Chinchilla et al. [2013] showed that the event exhibits signatures of deflection, which are usually associated with changes in the direction of propagation and/or rotation. The interaction with other magnetic obstacles could act as a catalyst of deflection or rotation effects. They also proposed a method to investigate the change of the ICME tilt based on analysis of height-time measurements. If this method is validated in future work, it may have important implications for space weather forecasting because it will allow the remote determination of complex ICME evolution in the inenr heliosphere.

2.3.3 Irregular ICMEs

Small transients (STs) have attracted considerable interest since they are frequently observed in the solar wind. The term "small" is defined as configurations whose passage at Earth may last from a few tens of minutes to a few hours. An important question is whether a possible relationship exists between these STs and the large-scale ICMEs/MCs.

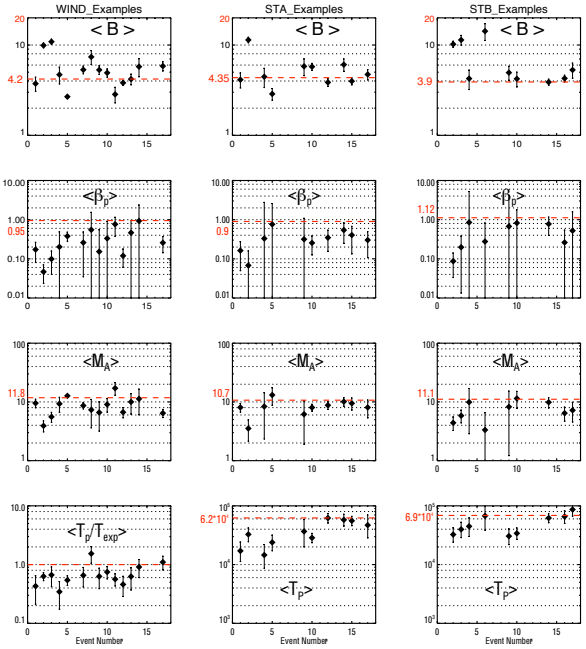

Figure 12: Statistical results on STs in March-April 2007: (i) average magnetic field strength, $\langle B \rangle$ [nT], (ii) proton beta, β_p, (iii) Alfvénic Mach number, M_A, and (iv) ratio of observed to expected proton temperature, T_p/T_{exp}. Data were taken from *Wind*, STEREO-A, and STEREO-B. Note that we only plot $\langle T_p \rangle$ [°K] for data from STEREO-A and STEREO-B. Figure adapted from *Yu et al.* [2014].

Yu et al. [2014] presented a comprehensive statistical analysis of STs in the solar minimum years 2007–2009. They looked at the 17 events, which occurred in March–April 2007. They showed scatterplots of the results obtained for the parameters (see Figure 12). The three columns refer, from left to right, to *Wind* (14 STs), STEREO-A (10 STs), and STEREO-B (9 STs) observations, respectively. Plotted in rows from top to bottom are averages of (a) $\langle B \rangle$, (b) β_p, (c) M_A, and (d) T_p/T_{exp}. For the STs observed by STEREO-A and STEREO-B, they compare the proton temperature T_p with the average values.

Comparing with ICMEs in the same solar minimum, they found the major difference to be that T_p in STs is not significantly less than the expected T_p. Thus, they summarized: (1) whereas a low T_p is generally considered a very reliable signature of ICMEs, it is not a robust signature of STs; and (2) since plasma $\beta \sim 1$, force-free modeling of STs having magnetic flux rope

geometry may be inappropriate.

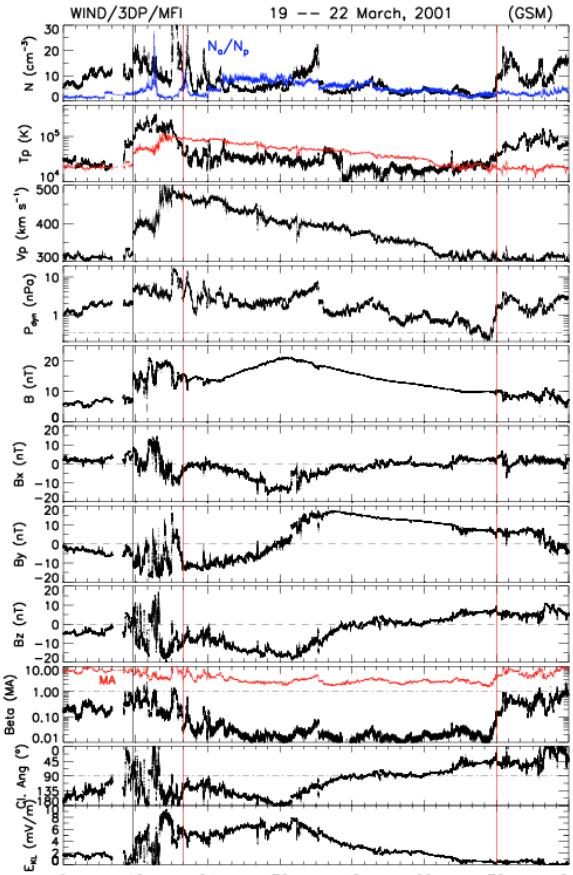

Figure 13: The 19-22 March, 2001 long-duration event. (top to bottom) The proton density (α-to-proton ratio in blue), the proton temperature (expected temperature in red), the velocity, dynamic pressure, magnetic field strength and magnetic field vector components in GSM coordinates, the plasma β (in red, the Alfvénic Mach number), and magnetic field clock angle, and the Kan-Lee reconnection electric field, E_{KL}. Figure adapted from *Lugaz and Farrugia* [2014].

In a recent CDAW workshop more than 50 CME-ICME pairs were investigated to understand why many CMEs originating close to the disk center of the Sun do not appear as flux ropes (magnetic clouds). It was shown based on charge state characteristics at 1 AU and flare characteristics at the Sun that all ICMEs are flux ropes, but the initial non radial motion at the Sun makes the CMEs appear as non-ropes [*Gopalswamy et al.*, 2013b; *Mäkelä et al.*, 2013; *Xie et al.*, 2013; *Yashiro et al.*, 2013]. CME deflections can be quite large, caused by polar coronal holes in the rise phase and equatorial coronal holes in the declining phase [*Gopalswamy*, 2015].

A significant fraction of transients observed by spacecraft at 1 AU do not show the well-defined properties of magnetic clouds (MCs). *Lugaz and Farrugia* [2014] proposed a new class of complex, non-magnetic cloud ejecta resulting from the interaction of two ICMEs with different orientations, which differ from previously studied multiple-MC events. At 1 AU, they are associated with a smooth rotation of the magnetic field vector over an extended duration and do not exhibit clear signs of interaction.

The characteristics of such events were first determined by *Lugaz and Farrugia* [2014] using numerical simulations. Then, a potential candidate, observed by *Wind* between March 19-22, 2001, was identified and analyzed (e.g., see Figure 13). Interestingly, the geomagnetic disturbances (e.g. substorms) stopped completely during the passage of the second ejecta when the clock angle was still 90°. Such events may result in intense, long-duration geomagnetic storms (in the March 2001 event Sym-H < -150 nT), with sawtooth substorms. They may sometimes be misidentified as isolated CMEs. This misidentification can adversely affect the accuracy of space weather predictions.

2.4 PSG#4: Dust Science

The charge released by impact ionization of fast dust grains impinging on spacecraft is at the basis of a well-known technique for dust detection by wave instruments. Since most of the impact charges are recollected by the spacecraft, monopole antennas generally detect a much greater signal than dipoles. This is illustrated by comparing dust signals in monopole and dipole modes on different spacecraft and environments. *Wind* observes micron-sized dust, both interplanetary dust (IPD) and interstellar dust (ISD), but its dipole antennas make detection of the IP nanodust discovered by STEREO/WAVES highly improbable. *Meyer-Vernet et al.* [2014] proposed an interpretation of the *Wind* dust data, elsewhere discussed by *Malaspina et al.* [2014], which explains the observed pulse amplitude and polarity for interstellar dust impacts, as well as the nondetection of nanodust. This proposed mechanism might be the dominant dust detection mechanism by some wave instruments using dipole antennas.

Malaspina et al. [2014] examined both the IPD and ISD populations observed by the electric field antennas from the *Wind* WAVES TDS receiver. The IPD population appears to vary on timescales as short as a day, or as long as a solar cycle. The 20+ year *Wind* data set could be used to explore the temporal evolution of the 1 AU dust environment. The ISD varies in flux and direction over 1-10 timescales consistent with model predictions.

Figure 14 shows monthly dust pseudo-count distributions where data for each month is averaged over 2006–2009. For each month, the averaged pseudocount distributions peak near the spacecraft ram direction, indicative of *Wind* encountering an approximately isotropic interplanetary dust population (technically, more retrograde dust is observed, but this may be a selection

effect). When the distribution peak is not in the ram direction, it is skewed toward the expected direction of ISD flow. When Earth's orbital velocity and interstellar flow velocity oppose in March, the relative velocity between *Wind* and the ISD reaches a maximum, leading to an increase in the number of measurable dust impacts. Near September, Earth's orbital velocity and the ISD velocity are nearly parallel and equal in magnitude, and ISD does not impact *Wind* with enough velocity to generate a signal. The data show diminished overall flux and a peak in the spacecraft orbital ram direction.

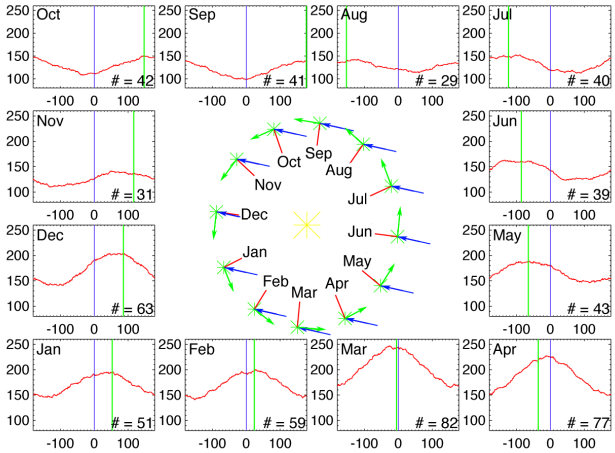

Figure 14: Monthly dust pseudo-count distributions where data for each month is averaged over 2006–2009. Horizontal axes indicate degrees clockwise from the expected ISD flow direction (258 degrees ecliptic longitude). Vertical axes are pseudocounts. Green lines indicate the ram direction of *Wind* about the Sun each month. Blue lines indicate the expected ISD flow direction. The number in the lower right of each plot indicates the difference between the maximum and minimum of that month's pseudocount distribution. The central figure shows the position of *Wind* (green star) about the Sun (yellow star) on the fifteenth day of each month. Green and blue lines retain their meanings. Red lines point sunward. Figure adapted from *Malaspina et al.* [2014].

These properties indicate that *Wind* observes primarily an isotropic interplanetary dust population at 1 AU, along with an interstellar dust component modulated by *Wind*'s velocity relative to the interstellar dust flow. **This data set contains information on the evolution of interstellar and interplanetary dust on day to solar cycle timescales. *Wind* is unique in that it is the only spacecraft where dust impact direction can be determined using measurements from an electric field instrument.**

2.5 Noteworthy Related Studies

Wind's unrivaled capabilities have led to a series of other studies that were not directly targeted in the previous Senior Review, but we felt were worth highlighting as they reflect the importance of *Wind* in the HSO.

In a number of studies, the Solar Physics group of Paris Observatory/LESIA has used radio observations over a broad wavelength range to trace the presence of energetic electrons in the corona. Several publications used *Wind*/WAVES data for this purpose. The presence or absence of type III bursts at decametric-hectometric (DH) frequencies is an especially useful tool to show if energetic electrons actually escape to the interplanetary space during solar eruptive events. Since the presence of a type III burst signals the presence of magnetic field lines that are open to interplanetary space, it is also likely to show that protons and ions accelerated in the corona get access to space. Thereby the time evolution of type III bursts can be used as a hint to diagnose the release of SEPs into space.

Trottet et al. [2014] investigated statistical relationships between the peak intensity of deka-hecto-keV electrons and deka-MeV protons observed near Earth between 1997 and 2006 and different measures of the importance of the associated solar activity. They showed that both CMEs and flares are quantitatively related to the intensity of the SEP events. *Wind*/WAVES data were essential to identify those solar events where flare-accelerated particles actually escaped to the interplanetary space. This identification was crucial to support the idea that the flare particles actually contribute to the SEPs observed near Earth.

Agueda et al. [2014] made detailed comparisons of the injection time histories of selected SEP events, as derived from the modeling of the interplanetary transport of electrons and protons, with electromagnetic emissions, particularly with DH type III radio bursts observed by *Wind*/WAVES. A correlation was found, which emphasizes the role that type III bursts can play in studying the access of energetic particles to space. This does not mean that all SEP injection signatures are accompanied by type III bursts: *Agueda et al.* [2014] identified SEP events with a long-lasting (> 1 hr) interval of solar release to space, but where type III bursts only occurred in the initial phase. The reason for the absence of type III bursts during the time-extended phases of particle acceleration is not entirely clear. One idea in the earlier literature is that when the particle acceleration proceeds gradually, the bump-on-the tail of the escaping electron distribution may not be sufficiently developed to give rise to pronounced type III burst emission. These time-extended acceleration phases are also accompanied by type IV continua at meter waves and by DH type II bursts emitted at coronal shock waves.

Klein et al. [2014] studied the release of relativistic protons to space during the large SEP event of 20 January 2005. The proton time profile as derived from neutron monitor observations on Earth exhibits two successive peaks. The onsets of both of them were ac-

companied by groups of type III bursts - one important argument that the two peaks of the proton profile were due to two successive episodes of particle acceleration in the solar corona. Through a detailed comparison of the proton time profile with a wide range of electromagnetic emissions, the study provided evidence that the two peaks were related to different episodes of magnetic reconnection in the solar corona, the first during the impulsive flare phase (this had actually been shown earlier by *Masson et al.* [2009]), and the second during the relaxation of the magnetically stressed corona after CME liftoff. No definite timing relationship was found between the periods of relativistic proton release and a type II bursts seen by *Wind*/WAVES during the late phase of the event.

The above studies suggest that particle acceleration in magnetic reconnection related to a flare and to the restructuring of the corona after CME liftoff does contribute to large SEP events seen at Earth, and their contribution may be increasingly important with increasing particle energy. The CME can be essential for SEP acceleration in two ways: acceleration of the particles at its shock wave, which seems particularly clear at moderate particle energies, and acceleration in the post-eruptive current sheet.

Wind/WAVES data related to SEP events were also integrated into the SEPServer database (European FP7 project), and are available together with quick look plots, at server.sepserver.eu. The project is described by *Vainio et al.* [2013], where also some preliminary investigations of the comparative timing of SEP release and DH type III bursts are discussed.

3 New Prioritized Science Goals

New Prioritized Science Goals

1. Long-term variations: 2 Full Solar Cycles
2. Solar wind structure
3. Kinetic signatures of heating and acceleration
4. Dust science

3.1 Two Full Solar Cycles

In November, 2016, within the time period covered by this proposal, *Wind* will complete 22 years, or one complete solar magnetic cycle, of continuous observations of the solar wind. Long-term solar cycle investigations always critically depend on continuous high quality observations, preferably from the same instruments to avoid instrument intercalibration issues. The *Wind* solar wind plasma and magnetic field data has shown a remarkable 0.1% stability due to the quality of the instruments and the intercalibration of SWE, 3DP and WAVES plasma frequency observations. The newly recalibrated MFI magnetic field data has also minimized any long-term drift effects. Thus the *Wind* solar wind observations will be very appropriate for comparing solar cycles 23 and 24.

The next few years offer us a unprecedented opportunity of using *Wind* data to investigate solar cycle variations of parameters characterizing the interplanetary medium (IPM) and how these variations influence the interaction of the solar wind with the terrestrial magnetosphere. *Wind* data will cover two complete solar cycles, comprised of three solar activity minima and two solar activity maxima. What is even more intriguing and worthy of investigation is that out of these, one was an abnormally weak and extended solar minimum (2007-2009), and another is the current weak solar activity maximum phase (2010–present).

There is a lot of interest in the community in such studies. Work has been done on these solar variations using *Wind* data. One approach has been to use the so-called "solar wind quasi-invariant" (QI), defined as the ratio of the magnetic-to-thermal energy densities (= inverse square of the Alfvén Mach number, M_A). Thus, QI characterizes the energy budget of the IPM.

In situ data has been used to model the QI in the solar wind [e.g., *Leitner et al.*, 2009, 2011] and specifically for magnetic clouds [e.g., *Leitner and Farrugia*, 2010; *Webb et al.*, 2012]. A further feature of solar activity is clearly reflected in the solar wind transients. These can be large–scale (ICMEs or Magnetic Clouds, MC) or small–scale, the latter appropriately called small transients (STs) [e.g., *Yu et al.*, 2014]. The frequency of large transients increases with solar activity. In contrast, STs have not been studied from this aspect. Such studies would advance our knowledge of the slow solar wind, of which, STs are believed to be an essential component.

The work by *Kilpua et al.* [2014], using *Wind* data, presents motivation for further investigation of the possible abnormalities of the recent solar minimum and maximum. Solar cycle 23 was the deepest and longest since the beginning of the space age. It had fewer strong and long-duration ICMEs which led to fewer geomagnetic storms.

Future work on these topics of solar cycle variations will extend these investigations along the following lines:

1. **STs:** solar cycle dependence; QI distribution; and relationship with slow solar wind
2. **Unusual Maximum:** compare geoeffects at Earth with other maxima; and quantify the weakness of the current maximum

Because Anomalous Cosmic Rays (ACRs) are primarily singly-ionized, comparisons with Galactic Cosmic Rays (GCRs) provide a means to untangle rigidity- and velocity-dependent effects in solar modulation.

The peak intensity of ACR N, O, Ne, and Ar appear at a few MeV/nucleon, an energy range that *Wind*/EPACT covers with geometry factor that is 10-50 times larger than instruments on ACE or STEREO. These new results can be compared to earlier *Wind*/EPACT ACR studies [e.g., *McDonald et al.*, 2010; *Reames*, 1999; *Reames and McDonald*, 2003; *Reames and Ng*, 2001] to **monitor the rise of ACRs at 1 AU during the unprecedented solar-modulation conditions in the declining phase of Solar Cycle 24**.

The declining phase of the Solar Cycle has generally produced the largest solar energetic particle (SEP) events of the cycle. *Wind*/EPACT, with a larger geometry factor, fills in energy gaps at ∼2-10 MeV/nucleon between instruments on ACE. *Wind*/EPACT also provides full-sky coverage, enabling detailed examination of evolving anisotropies that are unavailable from any other instrument. **Thus, we can examine differences in SEP events in the declining phase of Cycle 24.**

In addition, we can exploit the newly-developed technique of deriving the temperature of the source plasma of impulsive solar-energetic particles using systematic mass-to-charge ordering of heavy-ion enhancements [*Reames et al.*, 2014a,b]: Impulsive SEP events have small intensities and spectra that rarely extend beyond ∼10 MeV/nuc. The large geometry factor of the LEMT detector, part of *Wind*/EPACT, makes it uniquely able to measure the heavy-ion abundances with sufficient precision to extract temperatures. The ongoing LEMT observations of elements from the upper two-thirds of the periodic table are another unique contribution to these studies. When combined with already-published measurements, the new observations will be used to search for long-term temporal evolution in these temperatures, both through the course of Cycle 24 and in comparison with Cycle 23.

3.2 Solar Wind Structures

The solar wind is a highly structured medium. Besides long-term, solar cycle variations, hourly to daily variations correspond to various structures flying by the spacecraft. While solar cycle variations require long-term observations, multi-point observations are needed to identify and study the numerous solar wind transients. *Wind* will continue to participate in such studies in the upcoming years.

3.2.1 Coronal Mass Ejections

With the possible loss of teh STEREO-B spacecraft and as STEREO-A will round the sun coming closer to Earth during the time frame of this proposal, *Wind* will play an increasingly important role in identifying the global geometry of interplanetary coronal mass ejections, as *Wind* carries nearly ientcal magnetic field and thermal plasma instrumentation as STEREO.

In a recent study, *Möstl et al.* [2015] combined results from seven different heliospheric and planetary space missions (i.e., STEREO A & B, SOHO, SDO, *Wind*, *Mars Express*, and *Mars Science Laboratory*) to show why the CME on January 7, 2014, originally predicted to cause major disruptions, resulted in no significant geomagnetic effects. While the CME source region was almost at disk center facing Earth and the CME was very fast (3D speed of ∼2500 km/s), the eruption was strongly deflected in the corona and almost entirely missed Earth.

The CME's ecliptic part was deflected by $37 \pm 10°$ in heliospheric longitude, a value much larger than previously believed possible. These results will enhance our understanding of CME deflection and shape, which are fundamental ingredients for improving space weather forecasts.

In addition, working together with the three other L1 assets ACE, DSCOVR and SOHO, it will become possible to definitely identify drive shock and magnetic cloud boundary geometrical deformations. Previous three-point studies could not determine any deviations from strict planarity of these surfaces. **With the successful launch of DSCOVR, testing the predictions of numerical heliospheric models for structure deformation will be possible for the first time. *Wind* will play an important part in these multi-spacecraft studies.**

3.2.2 First Three-Point $B_\circ$ at L1

Even though a number of in-depth studies were carried out of solar wind correlation scale lengths using concurrent *Wind*, ACE, Soho and Genesis observations, only *Wind* and ACE have magnetometers, leaving the magnetic correlation question largely unanswered. The two STEREO spacecraft provided additional magnetic field measurements, but only for a very short period of time as they rapidly departed from the vicinity of Earth. The recently (February 2015) launched DSCOVR stationed also at L1, carries a fluxgate magnetometer nearly identical to those on ACE and *Wind*. Thus long-term and detailed three-point magnetic field intercomparison and correlation studies will become possible after the June 2015 commissioning of the DSCOVR spacecraft. It will become possible to test the hypothesis of *Collier et al.* [1998] derived from *Wind* and IMP 8 magnetic field observations, that the interplanetary magnetic field has a smaller correlation scale length than the solar wind plasma possibly identifying solar source structure sizes.

3.2.3 Tests of Turbulence Scale Lengths

The solar wind possesses variability also down at the minutes scale-length. Previous studies using multi-spacecraft observations with 10s to 100s of Re sepa-

ration could not uniquely separate time evolution and spatial size of these small turbulent solar wind structures. The *Wind*, ACE, DSCOVR and SOHO configuration, with variable separation distances, will for the first time able to identify the size and stability of these solar wind structures corresponding to the smallest observed photospheric features. These multi-spacecraft studies will be critical in determining how much 1 AU solar wind turbulent structures can reveal about the sources and acceleration of the solar wind.

3.3 Kinetic Signatures

The *Wind* spacecraft still retains some of the highest resolution measurements for near-Earth spacecraft, making it a unique observatory for tests of kinetic theory. Its capacity to measure electric and magnetic fields at high temporal cadence simultaneously with three-dimensional particle velocity distributions allows for tests applicable to future missions, such as *Solar Probe Plus*.

The *Wind* perigee passes through the Earth's plasmasphere gave *Issautier and Ongala* [2015] the opportunity to recently develop a systematic routine to determine the electron density, core and halo temperature and the magnitude of the magnetic field, based on Quasi-Thermal Noise spectroscopy method in Bernstein modes using the TNR radio instrument. A preliminary electron database was created to analyze the anti-correlation between electron density and temperature in this region. This type of analysis could help improve our estimates of the plasma properties of the cold plasma in the plasmasphere, which is often difficult to directly observe. **Such advancements will be beneficial for magnetospheric missions such as the *Van Allen Probes*, THEMIS, and MMS.**

3.3.1 Particle Heating and Acceleration

Recently *Wilson III et al.* [2012] showed, using *Wind* high time resolution observations, that electromagnetic waves in interplanetary shock ramps can simultaneously accelerate electrons and heat ions. These results identified a mechanism for energizing thermal particles up to suprathermal energies, thus providing the seed population required in many energetic particle acceleration theories. These results can also explain the heating of the corona and acceleration of electrons in solar flares.

These waves had not been observed in previous studies due to low time resolution measurements. The unique *Wind* high time resolution magnetic field and thermal particle observations combined with the newly processed and now publicly available search coil magnetometer data makes a systematic study of particle heating and acceleration at interplanetary shocks possible significantly extanding the case study of *Wilson III et al.* [2012]. **The resulting studies will pave the way for future *Solar Probe Plus* coronal science discoveries.**

3.3.2 Secondary Solar Wind Beams

The kinetic microstate of solar wind ions is the fingerprint of wave-particle interactions and fast dynamical processes. In non-collisional or otherwise weakly interacting solar wind plasmas, it can be an enduring indicator of the conditions accompanying a break from thermodynamic equilibrium in the corona shedding light on the origin mechanism itself (e.g. *Kasper et al.* [2013]). Under conditions where the solar wind is subject to shorter interaction timescales, non-Maxwellian microstates can be indicators of the transport mechanisms that govern or limit plasma energetics in situ.

In the last year, *Wind* researchers have developed tools and begun producing more sophisticated fits to the ion flux distributions measured by the *Wind* Faraday Cups on a large scale. Specifically, the presence and characteristics of proton and alpha beams with field-aligned drifts relative to the dominant core populations may be identified under a broad range of solar wind conditions.

In situ measurements of secondary proton populations in the inner heliosphere between 0.3 AU and 1 AU with Helios spacecraft [*Marsch et al.*, 1982b] indicated that proton beaming, typically between 0.8 and 2.0 times the locally measured Alfvn speed, was not uncommon in the solar wind. Later work demonstrated that the observed relative flow and beam strength could indicate an important limiting role played by proton-proton drift instabilities. Limitations of scope and access have rendered the Helios data set a tantalizing first peak into the rich phenomenology of ion-ion instabilities and associated plasma waves.

Wind scientists have recently fit the solar wind Faraday Cup spectra to model velocity distribution functions consisting of a bi-Maxwellian core and a secondary isotropic Maxwellian population in a systematic way, enabling a dramatic expansion of the work by *Marsch et al* and creating a deep resource for the study of ion drift instabilities. This analysis revealed that a significant secondary proton population has been present about a third of the time in the solar wind at 1 AU over the entire *Wind* mission. The majority of these secondary proton populations also exhibit magnetic field-aligned drifts at or near the local Alfvn speed relative to the core. The ubiquity of the configuration at 1 AU, particularly in the slow solar wind, has not to date been reported on or widely understood. The present analysis constitutes a nearly one thousand-fold increase in statistics on the subject.

Questions abound as to the origin and evolution of such microstates, with important implications for the

theory of solar wind transport, coronal heating, and perhaps for the reconnection of flux tubes. Are secondary beams a natural consequence of the coronal heating process? If secondary beams are limited to the local Alfvn speed by instabilities, how significant is the deceleration/diffusion of ion beams to the solar wind energy budget? Do unstable ion-ion states in the solar wind indicate topology changes or ongoing mixing of previously separate plasmas? If so, can they be used go better understand large scale structures? Can they be created in situ by wave-particle resonances or by reconnection of solar wind flux tubes? Can ion beam configurations be used to identify the operant mode in wave events observed in situ? **The increasingly sophisticated analysis of the Wind Faraday Cup data allows us to address the implications of proton double beaming in the coming years.**

3.4 More Dust Science

Motivated by the results found in the study by *Malaspina et al.* [2014], and others [e.g., *Meyer-Vernet et al.*, 2014], and the recent start of the MAVEN prime mission (which could detect dust using its electric field antennas), the importance of dust science in the community has risen. David Malaspina (PI) and L.B. Wilson III (Co-I) wrote an HGI-ODDE ROSES proposal, that was selected, to produce a dust impact database for the entire *Wind* mission. The specific science objectives that researchers can address with the creation of this database are: (1) Determine the effects of solar variability on the interaction between the heliosphere and interstellar medium; (2) Determine the timescales and mechanisms for variation in the $\sim$1 μm interplanetary dust near Earth; and (3) Maximize the science return of future missions like IMAP and Interstellar Probe.

The *Wind* data set is the only 20+ year long record of micron-sized IPD and ISD at 1 AU. And it is nearly unexplored. The results of recent work suggests that further study of dust observations recorded during *Wind*'s >20 year mission will lead to new insights concerning the characteristics and dynamics of the near-Earth IPD and ISD environment on multiple timescales, from days to entire solar cycles. Continuation of investigations into dust science will provide new understanding of the dust component of our solar system.

The interpretation of the so called "one hit" data points as nanodust on STEREO needs confirmation [e.g., *Zaslavsky et al.*, 2012], and such confirmation is ongoing with the *Wind* data. Some quandaries with the STEREO "one hit" interpretation are: "one hits" occur on only one STEREO antenna, even though the antennas are close together; on a given spacecraft, the antenna showing such "one hits" is always the same; the rate of "one hits" was different on the two STEREO spacecraft even when they were close together; and the rate on STEREO-Ahead has now reduced to zero. Further investigation with *Wind* may help to address these issues.

4 *Wind* Support for Current and Future Missions

As part of the Heliophysics System Observatory (HSO), *Wind* has been contributing to numerous science investigations that rely on multi-spacecraft observations. Many of these have been described in the preceding sections. In addition, *Wind* observations are also critical to many other spacecraft, enabling and enhancing their mission success. This section outlines some of these functions *Wind* serves.

4.1 ACE, DSCOVR, and STEREO

ACE

Wind and ACE have been mutually supporting each other in refining the calibrations of their instrumentation. Since *Wind* determines and inter-calibrates its solar wind plasma measurements from three different instruments that operate based on different physical principles (SWE, 3DP and WAVES), it supplies highly accurate and independent estimates of thermal plasma key parameters. In addition, the SWE instrument can operate through the high-energy particle showers associated with flares and CMEs. Thus the *Wind* data is very robust. The ACE SWEPAM team takes full advantage of these *Wind* solar wind plasma observations to improve their calibrations. This cooperation is expected to continue through the upcoming years.

Magnetic field measurement also mutually benefit from inter-calibrations between *Wind* and ACE. On spinning spacecraft, the highest accuracies are achieved for the spacecraft spin plane components. Since the *Wind* and ACE spin axes are perpendicular, the lower quality, spin axis component calibrations can be improved by comparing them to the appropriate spin plane component from the other spacecraft whenever they are sufficiently close to each other.

Finally, while ACE dominates high energy particle observations, the *Wind*/EPACT/LEMT telescope fills in an important gap in the 1-10 MeV/nucleon range between the ULEIS and SIS instruments on ACE. Since *Wind* is an ecliptic north spinner, unlike ACE detectors, the LEMT instrument also collects anisotropy information of the energetic particle distributions and can detect back-streaming populations from outer heliospheric shocks [e.g., *Tan et al.*, 2009]. Moreover, because of its large collecting area, EPACT can also measure the scientifically interesting smaller prompt solar energetic particle events. **In summary, *Wind* pro-**

vides significant calibration information to ACE, complements its measurements and facilitates collaborative, multi-spacecraft studies.

DSCOVR

The Deep Space Climate Observatory (DSCOVR) was launched on Feb. 11, 2015. DSCOVR is tasked to provide solar wind solar wind proton and magnetic field measurements from L1 (the same region where *Wind*, ACE and SoHO operate) for NOAA space weather prediction purposes. DSCOVR will accomplish this by two primary instruments: a Faraday Cup solar wind proton detector and a fluxgate magnetometer, both of which are derivatives of the equivalent instruments on *Wind*. Though DSCOVR is not a NASA science mission and the NOAA measurement requirements are not as strict as those for *Wind* and ACE, every effort will be made to process scientifically useful data from DSCOVR. To accomplish this, ***Wind* Faraday Cup and magnetometer data will be extensively used to intercalibrate the DSCOVR instruments** when the two spacecraft will be in close proximity.

Once fully calibrated, DSCOVR will provide even higher time cadence solar wind ion and magnetic field measurements than *Wind* can produce enabling two point studies of solar wind kinetic physics. For example, the size of reconnection exhausts and X-line current sheets can be determined. Also the special scale over which various wave-particle processes operate will be determined.

STEREO

With communications to STEREO-Behind currently interrupted and STEREO-Ahead soon to lose radio contact behind the sun, *Wind* will be the only inner heliosphere spacecraft with radio observations of the sun until late Dec., 2015 when STEREO-A is scheduled to return. Combined with the planned ending of MESSENGER and VEX, the importance of *Wind*'s in-situ measurements – that are very similar to those on STEREO-A – and their use in global heliospheric studies or testing of global heliospheric models have greatly increased. **Thus, *Wind* will remain a critical component for the HSO.**

4.2 MAVEN

The Mars Atmosphere and Volatile EvolutioN Mission (MAVEN), designed to study the Martian atmosphere, arrived at Mars (∼1.5 AU) on September 22, 2014. Mars will remain on the far side of the sun, relative to Earth, until early 2016. Thus, *Wind*, together with STEREO-A, will be an important element of this unique constellation providing in situ measurements of transients that can affect ≥120° of the inner heliosphere.

4.3 *Solar Probe Plus* and *Solar Orbiter*

Solar Probe Plus (SPP) and Solar Orbiter (SolO) are not planned to launch untill 2018, thus most of their primary mission is outside of the current proposal period. However, *Wind* already has and continues to perform significant studies aiding these future flagship missions. Only the high resolution of *Wind* measurements can provide appropriate 1 AU baseline for SPP and SolO observations; DSCOVR is expected to exhaust its propellant after ∼5 years while *Wind* has ∼60 years worth. SPP will have an 88 day orbit around the Sun, thus radial and magnetic alignment with *Wind* and with SolO in a 0.3-0.76 AU orbit will be frequent and these three-point studies will significantly enhance the science return of SPP and SolO.

SPP will be searching for physical processes that are responsible for the heating of the solar corona and the solar wind. These processes (e.g., instabilities, wave-particle interactions) tend to take place on very small time scales **near the Sun; barely resolvable even by the extremely high cadence SPP instruments. However, near 1 AU, the same processes operate at slightly lower time scales making their observation by *Wind* possible. Identifying which processes operate exclusively near the sun and which throughout the heliosphere will constrain theories of solar wind acceleration and heating, respectively.**

4.4 IBEX and *Voyagers*

Since the IMP 8 magnetometer stopped returning data in 2000, the *Wind* observations have usually supplied the 1 AU baseline for deep space observations such as those by the Voyagers. **The robust and continuous *Wind* solar wind measurements are essential for studies ranging from the predicted position of the termination shock and heliopause**, also observed remotely by IBEX, **to the evolution of solar wind transients from the inner heliosphere.**

4.5 Magnetospheric Missions

Nearly all magnetospheric investigations utilize, in some way, data from an upstream solar wind monitor. This is evidenced by the >1.7 million data access hits registered by CDAWeb for *Wind* and OMNI data (which largely relies upon *Wind* and ACE measurements) in 2013–2014. Missions that have, continue to, and will rely upon *Wind* for solar wind data include THEMIS, ARTEMIS, *Van Allen Probes* and MMS. Therefore, *Wind* will remain a crucial element in magnetospheric studies through the time covered by this senior review.

THEMIS

Two of the THEMIS spacecraft, called ARTEMIS, are now in permanent lunar orbits spending a large

fraction of their time in the ambient solar wind. *Wind*, together with the two ARTEMIS spacecraft, will provide unprecedented multi-point plasma measurements at the uniquely high, 3 second cadence that will address the fundamental question of whether the reconnection X-lines for low magnetic shears are generally patchy or extended. Multi-point high-resolution measurements with ARTEMIS will also be used to investigate the structure of the reconnection exhaust as a function of the distance from the X-line. It is worth noting that THEMIS used *Wind* to calibrate its thermal plasma instruments [*McFadden et al.*, 2008a,b], since its electric field receivers could not sample high enough frequencies to observe the upper hybrid line consistently.

***Van Allen Probes* and MMS**

The two *Van Allen Probes* launched on August 30, 2012 and the four MMS spacecraft are currently set to launch in mid 2015 (period covered by this Senior Review). In its detailed description of the scientific objectives for the mission, the *Van Allen Probes* Science Working Group has identified a need for solar wind observations to determine the occurrence patterns of the various acceleration, transport, and loss processes for relativistic, near-relativistic, and ring current particles within the Earth's inner magnetosphere. ***Wind* observations of the solar wind plasma and magnetic field will prove ideal for the required magnetospheric input measurements for the *Van Allen Probes* and for the MMS mission.**

4.6 RHESSI, *Swift*, and *Fermi*

RHESSI

RHESSI provides imaging and spectroscopy of the hard X-ray/γ-ray continuum and γ-ray lines emitted by energetic electrons and ions, respectively. RHESSI accurately locates these particles at the Sun, and its precise spectral measurements provide information on the spectra of the parent electrons and ions, and on the ion composition. *Wind*, using the 3DP and EPACT experiments, provides unique in-situ measurements of the energetic electrons and ions that reach ~1 AU, and, with WAVES, of the radio emissions produced by the energetic electrons while traveling from the Sun to 1 AU. Thus, *Wind* can provide a unique second remote observation point of flares on the sun and potentially an in-situ connection between radio bursts and the particles that generate them. *Wind* will continue to support this and similar RHESSI research projects.

Swift* and *Fermi

Cosmic gamma ray bursts (GRBs) are transients of large red-shift, and take place at least 600 times per year from the entire visible universe. GRBs have time durations of seconds or more, with photon energies ranging from the hard X-ray to very high energy γ-ray. Only 1 GRB is ever seen from any 1 source (since each is presumably a stellar birth/death signal).

Soft gamma repeaters (SGRs) are of somewhat less visible intensity, but with orders of magnitude less absolute magnitude, since their sources are in our Milky Way galaxy and its immediate neighbors, including the Magellanic Clouds. SGRs repeat at random, often or rarely, from a few times up to hundreds of times over spans from days to months. There are only half a dozen known SGR sources.

Giant Flares (GFs) are of greater apparent intensity than GRBs and are very rare, averaging once per decade. GFs are emitted from the source objects of the SGRs, one or none from each source, to date.

The KONUS instrument on *Wind* was designed to study GRBs, SGRs, and GFs, with omnidirectional sensitivity to all γ-ray transients. Its scientific data fall roughly into the following categories: KONUS detects on the average the brightest 120 GRBs per year, thus providing comparison data for many of the *Swift* GRBs. In particular, KONUS provides the higher energy determination that is beyond *Swift*'s energy range.

KONUS is also a key vertex in the Interplanetary GRB Network (IPN), composed of *Swift*, *Fermi*, *Mars Odyssey*, MESSENGER, INTEGRAL, AGILE, *Suzaku*, and HETE-2. The IPN finds the source directions of transients by virtue of its timing geometry, independently of oriented telescopes. KONUS is generally the most sensitive of these to SGRs, an advantage that result from its lack of collimation.

Finally, KONUS provides observations of GRBs for the Gamma-ray Coordinates Network (GCN), which contains the IPN, MAXI (on the ISS), and the MOA telescope in New Zealand. Due to the rarity of these astrophysical events, an additional four years of ***Wind* KONUS observations will significantly enhance the events collected by *Swift*, *Fermi*, the IPN, and the GCN.**

4.7 *Wind* and CCMC

The Coordinated Community Modeling Center (CCMC) is tasked to validate heliophysics models. In particular, Earth magnetospheric models are driven by solar wind input. The accuracy of this input especially during extreme solar wind conditions is critical for the proper evaluation of the models. Historically, *Wind* measurements have been used as the standard. It is expected that as future models will become more complex, their sensitivity to input uncertainties will only increase. **Thus continued *Wind* measurements are essential for the CCMC model validation program.**

4.8 *Wind* and CDAW Data Center

CDAW Data Center (cdaw.gsfc.nasa.gov) is a repository of CMEs and the associated phenomena related to space weather. The Data Center provides an online catalog of all CMEs identified manually from SOHO/LASCO images since 1996. There is also a catalog of all type II radio bursts observed by *Wind*/WAVES (Type II Radio Burst List) with links to the corresponding CMEs that produced the type II bursts. There also daily javascript movies that combine SOHO/LASCO images with *Wind*/WAVES dynamic spectra so that the connection between CMEs on the one hand and the radio bursts of type II, Type III, and type IV on the other can be identified (e.g. Dynamic Movie Creator). *Wind*/WAVES type II bursts have been shown to identify a small subset of CMEs important for space weather (Gopalswamy 2011). The *Wind*/WAVES observations are also linked to another catalog of CMEs producing SEP events because the same shocks cause type II bursts and accelerate protons.

5 Technical Status and Budget

5.1 Spacecraft Health

The *Wind* spacecraft continues in very good health. The communication system was successfully reconfigured in 2000 to realize an enhancement in telemetry margin. Reliance on a single digital tape recorder since the 1997 failure of the backup unit has never hampered operations, and measures were taken to minimize its use to extend its life. During the past few years, the spacecraft experienced a few instrument latch-ups and single bit flight software errors most likely due to high energy particle single event upsets. These events served to exercise the spacecraft and instrument recovery procedures and showed that within a day or two, all instruments can be brought back to full science operations.

On Oct. 27, 2014 (DOY 300) at 21:59:38 GMT, the *Wind* command and attitude processor (CAP1) suffered two single event upsets (SEUs). The redundant nature of *Wind* allowed the flight operations team (FOT) to successfully switch to a second CAP, CAP2. The spacecraft began returning data after the partial switch to CAP2 control on Nov. 7, 2014 (DOY 311). The FOT put CAP2 in full control on Nov. 20, 2014 (DOY 324), returning full functionality to all instruments. The SWE instrument, due to the SEUs, suffered a reset to safe mode. The instrument was reset to science mode and began returning house keeping data on Nov. 26, 2014 (DOY 330) and was returned to full functionality on Dec. 1, 2014 (DOY 335). SWE appears to be the only instrument directly affected by the CAP anomaly.

It was quickly determined that CAP2 had a hardware failure in its error encoding system. Thus, all data between Nov. 20, 2014 and Jan. 30, 2015 ∼17:50 UTC are subject to transmission errors, which occur at a rate of 1 bit error per ∼10000 bits (or 1 bit error per ∼1250 bytes). However, the spacecraft was still functioning at a data recovery rate >90%. Prior to the CAP anomaly, *Wind*'s average data recovery rate exceeded 97% for 2013 and 2014. For 2015, up to Jan. 18, 2015, *Wind*'s average data recovery rate was ∼97.5%.

The CAP anomaly resulted in a complete loss of data from Oct. 27, 2014 until Nov. 7, 2014 (11 days ∼ 3% annual total) and partial data loss from all instruments between Nov. 7, 2014 and Nov. 20, 2014 (24 days total ∼ 7% annual total). The SWE instrument suffered complete data loss from Oct. 27, 2014 to Nov. 26, 2014 (30 days ∼ 8% annual total) and partial loss (HK only) from Nov. 26, 2014 to Dec. 1, 2014 (35 days total ∼ 10% annual total).

On Jan. 21, 2015 the FOT reset CAP1 by removing both primary and secondary power (RAM and ROM resets failed) and began returning the CAP1 flight software. Between Jan. 28–30, 2015 the FOT returned CAP1 to full operational status, finalizing the work at ∼17:50 UTC on Jan. 30, 2015. During this recovery, the FOT switched control between CAP1 and CAP2. While CAP1 was in control, prior to its final recovery, the attitude/telemetry information was invalid for ∼4 hrs 41 mins, or < 5% of those four days.

An examination of the spacecraft power systems (see Figure 15) shows that the batteries can maintain average bias voltages high enough to exceed the current load shed setting until at least the year ∼2025 (extrapolated estimate from values in lower right-hand panel). In May 2012, all three batteries went through a mode change to reduce the maximum charge voltage (see lower-left-hand panel in Figure 15). Each battery was experiencing excess charging, causing an increase in temperature and reduction in efficiency. The successful mode changes reduced the temperatures to nominal ranges. At least two of the three batteries will require another mode change in 2015. At this rate – ∼3 years between mode changes – the batteries will last another ∼15–18 years since there are currently six more mode levels available.

The solar array output is producing more than enough current for spacecraft operations and will continue to do so well past the year ∼2018; assuming a requirement that a minimal current be drawn from the batteries (i.e., blue line in upper left-hand panel remains higher than red line in upper right). However, *Wind* operated for over a decade not satisfying the requirement until early 2012, when a more efficient sequence of commands were implemented during transmission. Under this less conservative requirement and

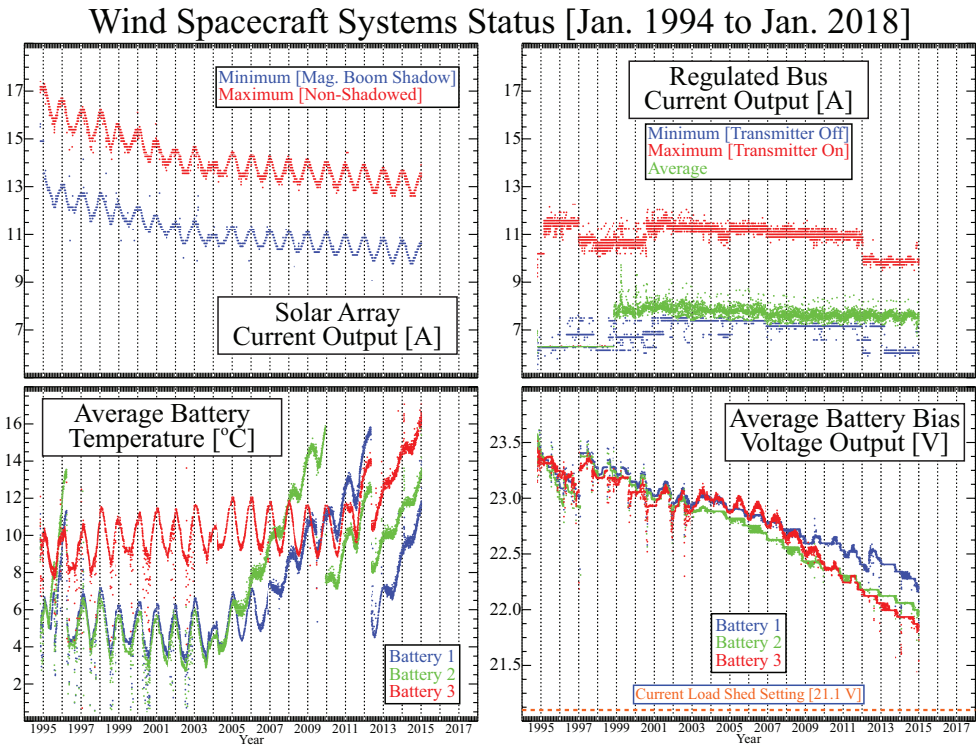

Figure 15: Summary of *Wind*'s Status: The *Wind* spacecraft systems status plotted from Jan. 1, 1994 to Jan. 1, 2018. The figure shows the solar panel array (upper left) current [Amp] output, regulated (upper right) bus current [Amp], average battery (lower left) temperatures [°C], and average battery (lower right) bias voltage [Volts] versus time. Each data point represents a daily average.

the current rate of degredation, the solar arrays would no longer meet the minimum current requirements for the regulated bus output by the year ∼2048 (i.e., when the blue line in upper left-hand panel drops below the green line in upper right). Therefore, *Wind* can operate at current capacity into the next decade.

Wind continues to have a large fuel reserve. The latest analysis shows that ∼55 kg fuel remains, which is equivalent of ∼106 m/s of radial delta-V assuming normal thruster operations. To maintain its current orbit around the L1 point, *Wind* needs to carry out four station keeping maneuvers every year. These maneuvers are very similar and require ∼0.5 m/s delta-V each. Thus, barring any other issues, *Wind* can maintain its orbit for nearly ∼53 years.

5.2 Instrument Status

Seven of the eight *Wind* instruments, including all of the fields and particles suits, remain largely or fully functional. The only instrument turned off is the TGRS γ-ray instrument that was designed for only a few years of operations. The general status of all instruments is summarized in Table 2.

The specific degradations in instrument capabilities are the following: The APE and IT detectors of the EPACT instrument, covering the highest energy ranges, do not work. The APE detector does return one channel of ∼20 MeV protons when enhanced. The LEMT and STEP telescopes of the same instrument continue to operate normally, providing crucial and unique observations of solar energetic particles up to 10 MeV in energy. On the SMS instrument the SWICS solar wind composition sensor had to be turned off in May 2000. The SMS DPU experienced a latch-up reset on 26 June 2009 that placed the MASS acceleration/deceleration power supply into a fixed voltage mode, rather than stepping through a set of voltages. It has been determined that a moderate risk power cycling of the SMS DPU would be required to fix this problem. In order to protect the unique and fully functional STICS sensor, it has been decided to leave the MASS sensor in a fixed voltage mode that allows reasonable but reduced science data collection. In 2010, MASS experienced a small degradation in the acceleration/deceleration power supply which reduced the efficiency of the instrument, though this does not seriously affect science data analysis.

The VEIS thermal electron detectors on the SWE instrument experienced high voltage problems in November, 2001. This problem was resolved by reprogramming the SWE Strahl sensor to recover most of the original functions. Moreover, the 3DP instrument also cov-

Table 2: The status of the *Wind* instruments

Instrument	Principal Investigator	Institution	Status
SWE	A.F- Viñas	Electrons: GSFC, UNH Ions: MIT, SAO	Strahl detector reconfigured Faraday Cup fully operational
3DP	S.D. Bale	UC Berkeley	Fully operational
MFI	A. Szabo	GSFC	Fully operational
SMS	S. Lepri	U. Michigan	SWICS turned off MASS reduced coverage STICS fully operational
EPACT	T. von Rosenvinge	GSFC	IT turned off APE – only 5 and 20 MeV protons LEMT and STEP operational
WAVES	R. MacDowall	GSFC	Fully operational
KONUS	E. Mazets	Ioffe Institute, Russia	Fully operational
TGRS	B. Teegarden	GSFC	Intentionally turned off (ran out of coolant)

ers the impacted electron measurements making these observations still redundant and hence robust. The entire SWE instrument suite required a full reset due to the CAP anomaly (see Section 5.1 for details), which resulted in a complete loss of data from late Oct. 27, 2014 to Nov. 26, 2014, and partial loss until Dec. 1, 2014 when the instrument was returned to nominal operations.

On May 2014 the 3DP instrument (specifically PESA Low) suffered an anomaly that only affected the telemetry house keeping (HK) data. A quick investigation showed that while the telemetry information (e.g., microchannel plate grid voltage) showed unreliable instrument operations information, the science data remained unaffected (i.e., no noticeable change in flux was observed during and after event). All the other detectors within the 3DP instrument suite continue to operate nominally. Thus, the anomaly resulted in no loss of scientific data.

Aside from the complete and partial data losses due to the CAP anomaly (see Section 5.1 for details), all of the instruments continue to be fully functional.

5.3 Science Team

The *Wind* instrument/science team is very small but an extremely dedicated group of scientists. Due to the longevity of the mission, a number of the original instrument PIs have retired or passed away. Keith Ogilvie passed the leadership of the SWE instrument suite to Adolfo Viñas and Justin Kasper (at University of Michigan) leading the SWE Faraday Cup team. Stuart Bale has taken over the PI-ship of 3DP at Berkeley. Adam Szabo is the PI for the MFI instrument. Sue Lepri (at the University of Michigan) is the PI for SMS. Though Tycho von Rosenvinge is still the PI for EPACT, Allan Tylka is playing an active role at Goddard to archive and distribute the data. Finally, Lynn Wilson is very active in the day-to-day operation of the mission as Deputy Project Scientist. The new team brings a great deal of experience and enthusiasm for new discoveries and data products, as evidenced by the long and increasing list of *Wind* scientific publications.

Students

Wind remains a very popular source of solar wind measurements and a rich source of material for Masters, PhD, and postdoctoral work. Since the last Senior Review, 8 students earned PhDs, 2 students earned Masters degrees, and 8 postdocs benefited from *Wind* observations. There are currently 14 PhD and 3 Masters students (of which we are aware) using *Wind* observations. The university team members also rely on a large number of undergraduate interns to increase their scientific productivity.

5.4 Ground Operations

Wind ground operations takes place at Goddard and is fully transitioned from the legacy *Polar*-*Wind*-*Geotail* system to Multi-Mission Operations Center (MMOC) that consolidates *Wind* operations with that of ACE. This transition became necessary with the decommissioning of *Polar* on April 30, 2008 and it includes the upgrade of outdated and costly to maintain hardware and software. *Wind* operations were moved to the MMOC on March 11, 2010 and the MMOC Operational Readiness Review was held on March 30, 2010.

For cost saving measures, the flight operations team reduced staffing by 1 FTE in November 2008 and modified shift schedules to reduce operational coverage from twelve to eight hours (reducing the need for overtime and shift differential). With the successful transition of *Wind* flight operations into the MMOC, the staffing levels have been reduced to operate the ACE and *Wind* missions with a combined team that also in-

cludes non-traditional flight operations skills (HW/SW maintenance, Flight Dynamics attitude analysis). Re-engineering/upgrading existing systems promoted efficiency with respect to implementing IT Security and HW/ SW maintenance as well as system administration. Automation is being implemented with a unified approach to further increase efficiency. The teams will continue to cross train at multiple positions so that prime and backup roles are covered. In spite of the disruptions due to the CAP anomaly, the data recovery rate for *Wind* for the years 2013 and 2014 averaged ∼96% (>97% prior to anomaly). Most of the unrecoverable data loss occurred when *Wind* Deep Space Network supports were released for other spacecraft launches and emergencies with some data loss resulting also from network problems.

The current operation of *Wind* requires one ∼2 hour DSN support per day. This allows the up-linking of the daily Stored Command Table load and the playback of the Digital Tape Recorder. *Wind* also maintains real-time solar wind monitoring during these 2 hour contacts. In 2001, an attempt was made to reduce the number of DSN contacts, and hence the cost of operations, by scheduling DSN time only once every three days, albeit for longer durations. Reducing the number of contacts saves the lengthy setup and reset times. After extensive testing it was concluded that this scenario did not provide significant savings and introduced critical risks to the mission. *Wind* can store only three days worth of commands, thus this is the longest *Wind* can go without ground contact or the spacecraft performs an emergency load shed. Hence the current flexibility to negotiate contact time with DSN would be eliminated. Also, all of these infrequent contacts would be fully attended regardless of the time of day. Currently about half of the contacts are completely automated allowing the operation staff to keep day schedules. Thus, the current daily contact scenario is considered optimal.

The automated distribution and archiving of level zero files and production of key parameter (KP) files also takes place at Goddard, but in the Science Directorate under the control of the project scientist. The two server (plus backup) system are periodically upgraded and maintained at modest cost.

5.5 In-Guide Budget

The in-guide budget described in this section will fund the mission operations necessary to continue the safe operation of the *Wind* spacecraft along with basic data reduction and validation processes performed at the various instrument institutions. As in the previous years, the scientific research outlined in the previous sections are expected to be funded through the Guest Investigator program with each element individually proposed and peer reviewed.

5.5.1 Mission Operations

The inputs in the budget spreadsheet Table II are the direct costs to the *Wind* project. Line 2b is Mission Services calculated by costing the flight operations team at a contractor WYE level of 7.2 for FY16 through FY20. Line 2b includes support from flight dynamics for orbit determination and station keeping maneuvers and the DSN scheduling work. The sustaining engineering cost for FY16–20 is for system administration of the MMOC. Line 2c represents the civil servant salary for a Mission Director, which is charged at 0.2 FTE.

Table IV provides the In Kind" costs. These are services provide to *Wind* that are funded by other sources. These costs are allocated to *Wind*, but are not supported with Project funds. Line 2a includes the use of the Deep Space Network apertures as well as the cost of voice and data connections at GSFC. Line 2b includes building engineers in the Mission Operations Building at GSFC and Mission Operations and Mission Services (MOMS) contract management costs.

Maintaining the *Wind* portion of the reengineered PWG system will require the support of a software engineer at the 0.2 FTE level. The PWG system is responsible for the archival of the level zero data and its distribution to the instrument sites and for the generation of the quick-look key parameter (KP) data files. Since this cost is directly funded from the *Wind* project funds, it is included in Table II line 3, Science Operations Functions. The aging PWG system hardware requires ∼$50K/year for FY16–FY20. This cost includes software license fees and are listed in Table III under LZ Production. The overall Goddard project management costs, not including the PWG system, include 0.5 FTE for the deputy project scientist and 0.2 FTE for a contract resource analyst, also carried in Table II on line 3. Note that ∼39% of the in-guide funding is needed for mission operations and only 8% for project management. Thus, more than half of the *Wind* budget still goes to the instrument teams for data processing and validation. The cost of the recent recovery of the *Wind* Command Attitude Processor (CAP1) by a heroic effort of the mission operations team, will be attempted to be absorbed in the existing small funding level.

5.5.2 Data Production and Accessibility

The *Wind* science data products are publicly served directly from the instrument team sites (most are directly available from CDAWeb), with a single project web page containing links to and descriptions of the large number of *Wind* data products (http://wind.nasa.gov). *Wind* is also an active participant in the development of the Virtual Heliophysics Observatory (VHO) that makes data queries even more user friendly and powerful. Details of the data production are given below.

The other half of the requested in-guide funding is allocated to the generation, calibration and validation of the various *Wind* instrument data products. After receiving the level zero instrument data along with housekeeping and ephemeris information, the instrument teams are responsible for the generation of science quality data that is fully calibrated and validated typically through the performance of well established scientific analysis. In addition, they have to provide full, data granule level description and intermediate-term archiving (i.e., guaranteed backups till final submission to SPDF/CDAWeb). In addition, the occasional *Wind* maneuvers (∼4/year for station keeping) necessitate instrument level commanding that the instrument teams are required to support. Thus, besides data production expertise, the teams have to maintain a low level engineering capability that can support routine and emergency operations. Finally, since *Wind* does not have a project level science center, the instrument teams are responsible for the public dissemination of their data through the maintaining of webpages.

Due to the limited funding available, the instrument teams optimized their operation to stay within ∼1 FTE for all aspects of operation. All fully functional instruments (MFI, SWE/Electron, SWE/Faraday Cup, WAVES, 3DP, and EPACT) are allocated almost exactly the same amount of support, regardless whether they are full cost accounted Goddard civil service or university operations. It should be noted that SWE is composed of two independent instruments: the Goddard electron instrument and the SAO/University of Michigan Faraday Cup. They each have the same allocation, but are reported together.

The partially functioning instrument (SMS) allocated about half as much as data production requirements are significantly diminished. However, it still continues to produce valuable data, therefore continued support at this reduced level is still requested. The astrophysical KONUS instrument receives no heliophysics funding. This instrument receives some minor amount of funding in Russia for data production and even less support from the Swift mission for a part time Goddard contractor. Thus, no new funding is requested for them in this proposal.

It should be also noted that for FY19 and FY20 a $200K overguide is requested to correct a typo in N2. The instructions to the *Wind* team was to program a fixed, $2.2M/year budget for these out years.

The current *Wind* project funding level does not allow any significant amount of funded science research and most of the results presented in this proposal were generated by independently funded teams. However, the core data calibration and validation work carried out by teh individual instrument teams does require an amount of science data analysis to verify teh accuracy of teh generated data products. Though it is difficult to be quantitative about teh fraction of work involved in this data validation work, an attempt was made to separate technical science operation functions and supporting science data analysis listed in Table II lines 3 and 4a. About 15% of the total *Wind* funding is devoted to this validation science data analysis or about a fifth of the non-mission operations funding.

References

Agueda, N., et al. (2014), Release timescales of solar energetic particles in the low corona, *Astron. & Astrophys.*, *570*, A5, doi:10.1051/0004-6361/201423549.

Bougeret, J.-L., et al. (1995), Waves: The Radio and Plasma Wave Investigation on the Wind Spacecraft, *Space Sci. Rev.*, *71*, 231–263, doi:10.1007/BF00751331.

Chen, C. H. K., et al. (2014), Ion-scale spectral break of solar wind turbulence at high and low beta, *Geophys. Res. Lett.*, *41*, 8081–8088, doi:10.1002/2014GL062009.

Cliver, E. W., et al. (2013), Solar Drivers of 11-yr and Long-Term Cosmic Ray Modulation, *Space Sci. Rev.*, *176*, 3–19, doi:10.1007/s11214-011-9746-3.

Collier, M. R., et al. (1998), Timing accuracy for the simple planar propagation of magnetic field structures in the solar wind, *Geophys. Res. Lett.*, *25*, 2509–2512, doi:10.1029/98GL00735.

Farrell, W. M., et al. (1995), A method of calibrating magnetometers on a spinning spacecraft, *IEEE Trans. Mag.*, *31*, 966–972, doi:10.1109/20.364770.

Farrugia, C. J., et al. (2014), A Vortical Boundary Layer for Near-Radial IMF: Wind Observations on October 24, 2001, *J. Geophys. Res.*, *119*, 4572–4590, doi:10.1002/2013JA019578.

Feldman, W. C., et al. (1974), The solar wind He^{2+} to H^+ temperature ratio, *J. Geophys. Res.*, *79*, 2319, doi:10.1029/JA079i016p02319.

Ghielmetti, A. G., et al. (1983), Calibration system for satellite and rocket-borne ion mass spectrometers in the energy range from 5 eV/charge to 100 keV/charge, *Rev. Sci. Inst.*, *54*, 425–436, doi:10.1063/1.1137411.

Gloeckler, G., et al. (1995), The Solar Wind and Suprathermal Ion Composition Investigation on the Wind Spacecraft, *Space Sci. Rev.*, *71*, 79–124, doi:10.1007/BF00751327.

Gopalswamy, N. (2015), The Dynamics of Eruptive Prominences, in *Astrophysics and Space Science Library*, *Astrophysics and Space Science Library*, vol. 415, edited by J.-C. Vial and O. Engvold, p. 381, doi:10.1007/978-3-319-10416-4_15.

Gopalswamy, N., et al. (2013a), Testing the empir-

ical shock arrival model using quadrature observations, *Space Weather*, *11*, 661–669, doi:10.1002/2013SW000945.

Gopalswamy, N., et al. (2013b), The Solar Connection of Enhanced Heavy Ion Charge States in the Interplanetary Medium: Implications for the Flux-Rope Structure of CMEs, *Solar Phys.*, *284*, 17–46, doi:10.1007/s11207-012-0215-2.

Gopalswamy, N., et al. (2014), Anomalous expansion of coronal mass ejections during solar cycle 24 and its space weather implications, *Geophys. Res. Lett.*, *41*, 2673–2680, doi:10.1002/2014GL059858.

Hefti, S., et al. (1998), Kinetic properties of solar wind minor ions and protons measured with SOHO/CELIAS, *J. Geophys. Res.*, *103*, 29,697–29,704, doi:10.1029/1998JA900022.

Hellinger, P., et al. (2011), Heating and cooling of protons in the fast solar wind between 0.3 and 1 AU: Helios revisited, *J. Geophys. Res.*, *116*, 9105, doi:10.1029/2011JA016674.

Huba, J. D. (2011), Nrl plasma formulary, *Tech. Rep. NRL/PU/6790–11-551*, Naval Research Laboratory, Washington, DC 20375-5320.

Issautier, K., and S. Ongala (2015), QuasiThermal Noise in Bernstein modes based on Wind perigees in Earth magnetosphere, *Geophys. Res. Lett.*, in preparation.

Kasper, J. C., et al. (2006), Physics-based tests to identify the accuracy of solar wind ion measurements: A case study with the Wind Faraday Cups, *J. Geophys. Res.*, *111*, 3105–+, doi:10.1029/2005JA011442.

Kasper, J. C., et al. (2008), Hot Solar-Wind Helium: Direct Evidence for Local Heating by Alfvén-Cyclotron Dissipation, *Phys. Rev. Lett.*, *101*, 261,103–+, doi:10.1103/PhysRevLett.101.261103.

Kasper, J. C., et al. (2013), Sensitive Test for Ion-Cyclotron Resonant Heating in the Solar Wind, *Phys. Rev. Lett.*, *110*(9), 091102, doi:10.1103/PhysRevLett.110.091102.

Kilpua, E. K. J., et al. (2014), Why have geomagnetic storms been so weak during the recent solar minimum and the rising phase of cycle 24?, *J. Atmos. Solar-Terr. Phys.*, *107*, 12–19, doi:10.1016/j.jastp.2013.11.001.

Klein, K.-L., et al. (2014), The relativistic solar particle event of 2005 January 20: origin of delayed particle acceleration, *Astron. & Astrophys.*, *572*, A4, doi:10.1051/0004-6361/201423783.

Koval, A., and A. Szabo (2008), Modified "Rankine-Hugoniot" shock fitting technique: Simultaneous solution for shock normal and speed, *J. Geophys. Res.*, *113*, 10,110–+, doi:10.1029/2008JA013337.

Leitner, M., and C. J. Farrugia (2010), Solar wind quasi invariant within ICMEs, *Proc. 12th Intl. Solar Wind Conf.*, *1216*, 652–654, doi:10.1063/1.3395951.

Leitner, M., et al. (2009), The Solar Wind Quasi-Invariant Observed by STEREO A and B at Solar Minimum 2007 and Comparison with Two Other Minima, *Solar Phys.*, *259*, 381–388, doi:10.1007/s11207-009-9412-z.

Leitner, M., et al. (2011), Change of solar wind quasi-invariant in solar cycle 23–Analysis of PDFs, *J. Atmos. Solar-Terr. Phys.*, *73*, 290–293, doi:10.1016/j.jastp.2010.03.002.

Lepping, R. P., et al. (1995), The Wind Magnetic Field Investigation, *Space Sci. Rev.*, *71*, 207–229, doi:10.1007/BF00751330.

Lin, R. P., et al. (1995), A Three-Dimensional Plasma and Energetic Particle Investigation for the Wind Spacecraft, *Space Sci. Rev.*, *71*, 125–153, doi:10.1007/BF00751328.

Lugaz, N., and C. J. Farrugia (2014), A new class of complex ejecta resulting from the interaction of two CMEs and its expected geoeffectiveness, *Geophys. Res. Lett.*, *41*, 769–776, doi:10.1002/2013GL058789.

Mäkelä, P., et al. (2013), Coronal Hole Influence on the Observed Structure of Interplanetary CMEs, *Solar Phys.*, *284*, 59–75, doi:10.1007/s11207-012-0211-6.

Malandraki, O. E., et al. (2012), Scientific Analysis within SEPServer – New Perspectives in Solar Energetic Particle Research: The Case Study of the 13 July 2005 Event, *Solar Phys.*, *281*, 333–352, doi:10.1007/s11207-012-0164-9.

Malaspina, D. M., et al. (2014), Interplanetary and interstellar dust observed by the Wind/WAVES electric field instrument, *Geophys. Res. Lett.*, *41*, 266–272, doi:10.1002/2013GL058786.

Marsch, E., et al. (1982a), Solar wind helium ions - Observations of the HELIOS solar probes between 0.3 and 1 AU, *J. Geophys. Res.*, *87*, 35–51, doi:10.1029/JA087iA01p00035.

Marsch, E., et al. (1982b), Solar wind protons - Three-dimensional velocity distributions and derived plasma parameters measured between 0.3 and 1 AU, *J. Geophys. Res.*, *87*, 52–72, doi:10.1029/JA087iA01p00052.

Maruca, B. A., and J. C. Kasper (2013), Improved interpretation of solar wind ion measurements via high-resolution magnetic field data, *Adv. Space Res.*, *52*, 723–731, doi:10.1016/j.asr.2013.04.006.

Maruca, B. A., et al. (2013), Collisional Thermalization of Hydrogen and Helium in Solar-Wind Plasma, *Phys. Rev. Lett.*, *111*(24), 241101, doi:10.1103/PhysRevLett.111.241101.

Masson, S., et al. (2009), Acceleration of Relativistic Protons During the 20 January 2005 Flare and CME, *Solar Phys.*, *257*, 305–322, doi:10.1007/s11207-009-9377-y.

McComas, D. J., et al. (2013), Weakest Solar Wind of the Space Age and the Current "Mini" Solar Maximum, *Astrophys. J.*, *779*, 2, doi:10.1088/0004-637X/779/1/2.

McDonald, F. B., et al. (2010), Unusual time histories of galactic and anomalous cosmic rays at 1 AU over the deep solar minimum of cycle 23/24, *Geophys. Res. Lett.*, *37*, L18101, doi:10.1029/2010GL044218.

McFadden, J. P., et al. (2008a), The THEMIS ESA Plasma Instrument and In-flight Calibration, *Space Sci. Rev.*, *141*, 277–302, doi:10.1007/s11214-008-9440-2.

McFadden, J. P., et al. (2008b), THEMIS ESA First Science Results and Performance Issues, *Space Sci. Rev.*, *141*, 477–508, doi:10.1007/s11214-008-9433-1.

McIntosh, S. W., et al. (2015), The Solar Magnetic Activity Band Interaction and Instabilities that Shape Quasi-Periodic Variability, *Nature Comm.*, in press.

Meyer-Vernet, N., et al. (2014), The importance of monopole antennas for dust observations: Why Wind/WAVES does not detect nanodust, *Geophys. Res. Lett.*, *41*, 2716–2720, doi:10.1002/2014GL059988.

Möstl, C., et al. (2014), Connecting Speeds, Directions and Arrival Times of 22 Coronal Mass Ejections from the Sun to 1 AU, *Astrophys. J.*, *787*, 119, doi:10.1088/0004-637X/787/2/119.

Möstl, C., et al. (2015), Strong coronal deflection of a solar storm and its interplanetary evolution to Earth and Mars, *Nature Comm.*, submitted Jan 14, 2015.

Muzamil, F. M., et al. (2014), Structure of a reconnection layer poleward of the cusp: Extreme density asymmetry and a guide field, *J. Geophys. Res.*, *119*(9), 7343–7362, doi:10.1002/2014JA019879.

Neugebauer, M. (1976), The role of Coulomb collisions in limiting differential flow and temperature differences in the solar wind, *J. Geophys. Res.*, *81*, 78–82, doi:10.1029/JA081i001p00078.

Nieves-Chinchilla, T., et al. (2013), Inner Heliospheric Evolution of a "Stealth" CME Derived from Multiview Imaging and Multipoint in Situ observations. I. Propagation to 1 AU, *Astrophys. J.*, *779*, 55, doi:10.1088/0004-637X/779/1/55.

Ogilvie, K. W., et al. (1995), SWE, A Comprehensive Plasma Instrument for the Wind Spacecraft, *Space Sci. Rev.*, *71*, 55–77, doi:10.1007/BF00751326.

Pulupa, M. P., et al. (2014), Core Electron Heating in Solar Wind Reconnection Exhausts, *Astrophys. J. Lett.*, *791*, L17, doi:10.1088/2041-8205/791/1/L17.

Reames, D. V. (1999), Quiet-Time Spectra and Abundances of Energetic Particles During the 1996 Solar Minimum, *Astrophys. J.*, *518*, 473–479, doi:10.1086/307255.

Reames, D. V. (2013), The Two Sources of Solar Energetic Particles, *Space Sci. Rev.*, *175*, 53–92, doi:10.1007/s11214-013-9958-9.

Reames, D. V. (2014), Element Abundances in Solar Energetic Particles and the Solar Corona, *Solar Phys.*, *289*, 977–993, doi:10.1007/s11207-013-0350-4.

Reames, D. V., and F. B. McDonald (2003), Wind Observations of Anomalous Cosmic Rays from Solar Minimum to Maximum, *Astrophys. J. Lett.*, *586*, L99–L101, doi:10.1086/374653.

Reames, D. V., and C. K. Ng (2001), On the Phase of the 27 Day Modulation of Anomalous and Galactic Cosmic Rays at 1 AU during Solar Minimum, *Astrophys. J. Lett.*, *563*, L179–L182, doi:10.1086/338654.

Reames, D. V., et al. (2014a), Variations in Abundance Enhancements in Impulsive Solar Energetic-Particle Events and Related CMEs and Flares, *Solar Phys.*, *289*, 4675–4689, doi:10.1007/s11207-014-0589-4.

Reames, D. V., et al. (2014b), Abundance Enhancements in Impulsive Solar Energetic-Particle Events with Associated Coronal Mass Ejections, *Solar Phys.*, *289*, 3817–3841, doi:10.1007/s11207-014-0547-1.

Richardson, I. G., et al. (2014), > 25 MeV Proton Events Observed by the High Energy Telescopes on the STEREO A and B Spacecraft and/or at Earth During the First $\sim$ Seven Years of the STEREO Mission, *Solar Phys.*, *289*, 3059–3107, doi:10.1007/s11207-014-0524-8.

Schmidt, W. K. H., et al. (1980), On temperature and speed of He/2+/ and O/6+/ ions in the solar wind, *Geophys. Res. Lett.*, *7*, 697–700, doi:10.1029/GL007i009p00697.

Schwadron, N. A., et al. (2014), Coronal electron temperature in the protracted solar minimum, the cycle 24 mini maximum, and over centuries, *J. Geophys. Res.*, *119*, 1486–1492, doi:10.1002/2013JA019397.

Tan, L. C., et al. (2009), Observational Evidence on the Presence of an Outer Reflecting Boundary in Solar Energetic Particle Events, *Astrophys. J.*, *701*, 1753–1764, doi:10.1088/0004-637X/701/2/1753.

Trottet, G., et al. (2014), Statistical Evidence for Contributions of Flares and Coronal Mass Ejections to Major Solar Energetic Particle Events, *Solar Phys.*, doi:10.1007/s11207-014-0628-1.

Vainio, R., et al. (2013), The first SEPServer event catalogue $\sim$68-MeV solar proton events observed at 1 AU in 1996-2010, *J. Space Weather Space Climate*, *3*(26), A12, doi:10.1051/swsc/2013030.

von Rosenvinge, T. T., et al. (1995), The Energetic Particles: Acceleration, Composition, and Transport (EPACT) investigation on the WIND spacecraft, *Space Sci. Rev.*, *71*, 155–206, doi:10.1007/BF00751329.

von Steiger, R., et al. (1995), Kinetic Properties of Heavy Ions in the Solar Wind From SWICS/Ulysses,

Space Sci. Rev., *72*, 71–76, doi:10.1007/BF00768756.

Webb, A., et al. (2012), Solar Wind Quasi-invariant for Slow and Fast Magnetic Clouds, *Solar Phys.*, *277*, 375–388, doi:10.1007/s11207-011-9904-5.

Wicks, R. T., et al. (2013), Correlations at Large Scales and the Onset of Turbulence in the Fast Solar Wind, *Astrophys. J.*, *778*, 177, doi:10.1088/0004-637X/778/2/177.

Wilson III, L. B., et al. (2012), Shocklets, SLAMS, and field-aligned ion beams in the terrestrial foreshock, *Geophys. Res. Lett.*, doi:10.1029/2012GL050958, rejected.

Xie, H., et al. (2013), Near-Sun Flux-Rope Structure of CMEs, *Solar Phys.*, *284*, 47–58, doi:10.1007/s11207-012-0209-0.

Yashiro, S., et al. (2013), Post-Eruption Arcades and Interplanetary Coronal Mass Ejections, *Solar Phys.*, *284*, 5–15, doi:10.1007/s11207-013-0248-1.

Yu, W., et al. (2014), A Statistical Analysis of Properties of Small Transients in the Solar Wind 2007-2009: STEREO and Wind Observations, *J. Geophys. Res.*, *119*(2), 689–708, doi:10.1002/2013JA019115.

Zaslavsky, A., et al. (2012), Interplanetary dust detection by radio antennas: Mass calibration and fluxes measured by STEREO/WAVES, *J. Geophys. Res.*, *117*, 5102, doi:10.1029/2011JA017480.

A Mission Archive Plan

Early in its mission, *Wind* and the other GGS spacecraft relied on a very capable and extensive science operations center, the Science Planning and Operations Facility (SPOF). The SPOF was responsible for the collecting, distribution and active archiving of all level zero (LZ) and ancillary data products. The SPOF also ran daily the instrument team provided data processing software to produce quick turnaround, publicly available data, termed Key Parameters (KPs). The SPOF also provided science planning and software maintenance services.

With the passage of time, and with reducing funding levels, the SPOF had to be turned off and most of its functions were passed on to the instrument teams and to a small operation, the *Polar*-*Wind*-*Geotail* (PWG) system, that continued to perform some LZ and KP functions. This unavoidable decentralization resulted in a degree of unevenness and disparity between the various *Wind* instrument data services. To solve this problem, key *Wind* instrument team members rallied around the new distributed Heliophysics Data Environment (HDE) concept and became funding members of the Virtual Heliospheric Observatory (VHO). The VHO provides a single point of entry for data location without the costly necessity of a dedicated science operations center. As a byproduct, *Wind* instrument data were among the first to be fully documented with the common SPASE dictionary based metadata standard thus providing the user community an even level of descriptions of instruments and data products.

Mission Operations Center

Wind ground operations takes place at Goddard and is fully transitioned from the legacy system to Multi-Mission Operations Center (MMOC) that consolidates *Wind* operations with that of ACE. This transition became necessary with the decommissioning of *Polar* on April 30, 2008 and it includes the upgrade of outdated and costly to maintain hardware and software. *Wind* operations were moved to the MMOC on March 11, 2010 and the MMOC Operational Readiness Review was held on March 30, 2010.

The primary responsibility of the MMOC is spacecraft commanding, trend and anomaly analysis, DSN scheduling, the maintenance of *Wind* Near-Real-Time (NRT) passes and LZ generation for each instrument and spacecraft housekeeping. In addition, the Goddard Flight Dynamics Facility provides orbit solutions to the MMOC. The MMOC, in turn, sends all of these data products daily to the PWG system.

The PWG System

The PWG system handles the active archiving of LZ and ancillary files and their distribution to the instrument teams and various active archives. The PWG system also performs the rapid KP data production for all instruments. It resides also at Goddard but with the team of the project scientist. The PWG system has been streamlined onto only two computers (a data server and a data processor, with hot spares) and is fully automated to eliminate the need for data technicians. The system is maintained by one civil service IT engineer at a fraction of FTE. This system also serves as the interface to the *Wind* NRT data stream, which is real-time processed data during the daily ∼2 hour long spacecraft telemetry contact times. This NRT data is available in numerical and graphical format at: http://pwg.gsfc.nasa.gov/windnrt/.

The PWG system distributes the instrument and spacecraft housekeeping LZ files to the instrument teams via FTP. All of these LZ and orbit/attitude files are also publicly accessible at ftp://pwgdata.gsfc.nasa.gov/pub/. Only the most recent 60 days are served in uncompressed format, but the whole mission is archived in GZip compression. Even though the deep archival of these data files are handled by SPDF, the PWG system also backs up all LZ data at two physical locations and onto CDAWeb. It should be noted that the whole *Wind* mission to date requires only 300GB of storage for the LZ data, so the backup requirements are not overwhelming.

At the beginning of the mission, all *Wind* instrument teams had to supply software to automatically process some portion of their data into science data products, the Key Parameter (KP) data. Even though the KP data is clearly not the best quality data the instrument teams produce, because it is always available publicly within 24 hours of observation, it enjoys great popularity. The PWG system maintains this software library, with occasional support (as needed) from the instrument teams and automatically places all the KP data on http://cdaweb.gsfc.nasa.gov. A more detailed description of the various KP products is given at the instrument sections below.

The PWG system also keeps the Satellite Situation Center (SSCWeb) up to date with orbit information (http://sscweb.gsfc.nasa.gov). Thus, all orbit graphics generated on SSCWeb are always up to date.

Instrument Data

The bulk of the instrument data dissemination takes place through CDAWeb that also serves as the *Wind*

Active Archive. To aid the user community, we also developed a *Wind* project web page (http://wind.nasa.gov) that identifies the entry point for each instrument data environment and provides some degree of common documentation. The *Wind* project web page includes an updated list of publications and a link to the *Wind* Wikipedia web page (http://en.wikipedia.org/wiki/WIND_(spacecraft)) that we developed. Most of the *Wind* data products can also be searched, down to the parameter level, through VHO providing rapid access to a wide range of events in the very long duration *Wind* data set. Next we detail the data product status of each *Wind* instrument.

SWE Ions

Documentation: The SWE Faraday Cup (FC) sub-system was designed to measure solar wind thermal protons and positive ions. The physical sensor is completely described in the Space Science Review article *Ogilvie et al.* [1995]. This article was also reproduced in the Global Geospace Mission book and portions of it are available through the *Wind* project web page (http://wind.nasa.gov).

The data production procedures are described by *Ogilvie et al.* [1995], but a much more detailed discussion is provided by J.C. Kasper in his PhD dissertation. The relevant chapters are reproduced on the *Wind* project web page. While error analysis results are included in each FC data file, the systematic uncertainties of the measurements, calibrated against other *Wind* instruments and based on basic physical principles, are discussed in *Kasper et al.* [2006]. This paper is also available on the *Wind* project web page.

Data Products: The PWG system, on receipt of the LZ data, immediately processes a KP data product for SWE/FC. This automated procedure uses a convected isotropic Maxwellian to fit to the reduced distribution functions collected by the FC. These 92-second time resolution ASCII data files are available to the public within 24 hours of the observations at the MIT instrument web site (http://web.mit.edu/space/www/wind/wind_data.html) and at CDAWeb (http://cdaweb.gsfc.nasa.gov). One hour averages of this data is also available at the MIT instrument page. While the KP products were originally designed as browse, quick look data, the quality proved to be so high that this data product became a frequently used science level data product of the FC sub-system.

A data production algorithm was developed that employs a bi-Maxwellian fit and obtains anisotropic temperatures for protons and a separate fit for Alpha particles. The resulting data product (designated H1 by CDAWeb), also contains the simpler moment computations primarily to allow direct comparison with the ACE SWEPAM proton data. This 92-second time resolution data can be located in CDF format at CDAWeb. The whole mission, since 1994 has been reprocessed with this new algorithm and is available generally till 2-3 months behind real time as it requires the final calibrated MFI magnetic field data that needs several months to be computed.

SWE Ion Data	Cadence	Coverage	Format	Location
KP Protons (K0)	92 s	1994/11/17–Present	ASCII CDF	MIT[a], FTPHelper[b] CDAWeb[c]
KP Protons	1 hr	1994/11/17–Present	ASCII	MIT
Bi-Maxwellian (H1)	92 s	1995/01/01–Present[d]	ASCII CDF	MIT CDAWeb
Reduced Velocity Distributions (SW-ION-DIST)	92 s	1994/11/15–Present	CDF	CDAWeb

[a] http://web.mit.edu/space/www/wind/wind_data.html; [b] http://ftpbrowser.gsfc.nasa.gov;
[c] http://cdaweb.gsfc.nasa.gov; [d] ∼6 month lag

A new data product, designated WI_SW-ION-DIST_SWE-FARADAY, was released in March 2014 containing the reduced velocity distribution functions for the two FCs. It is a high-level data set that provides positive ion charge flux as measured by the Solar Wind Experiment (SWE) Faraday Cups on board the *Wind* spacecraft. These data span the duration of the experiment, from November 15, 1994 through the present release. Charge flux measurements (pA) are organized into spectra as a function of angle (degrees) and energy-per-charge (V). Each spectrum consists of 20 azimuth angles, 2 zenith angles (cup 1 and cup 2), and 31 energy-per-charge windows, for a total of 1240 independent measurements per spectrum. Spectra are provided at approximately 92-second intervals, ordered by the epoch time (ms) at the beginning of each measurement interval. A lookup table is provided for the effective area of the sensor as a function of incidence angle. The data files are indexed by day.

It is also possible to obtain special proton beam fits on request from Michael Stevens (e-mail: msteven-scfa.harvard.edu) at the Harvard Center for Astrophysics. These fits are specialized in that they only treat events where there is an extra proton beam, in addition to the usual proton solar wind core and associated alpha-particle beam. The occurrence rate of such events is low enough to limit this data product on an event-by-event basis. However, the availability of such a product is very important as it allows for tests of ion/ion instabilities.

Two new FC data products are being considered for development. The first is analogous to the H1 data product, but it utilizes the higher time resolution MFI data for each spacecraft rotation. The details can be found in *Maruca and Kasper* [2013]. The advantage would be to reduce aliasing introduced by using a 92 s average of the magnetic field. The main impact is that the original method consistently underestimated the temperature anisotropy of the ions.

The second new data product is an open-source Python GUI being developed by Bennet Maruca under NASA ROSES grants. The GUI would allow users to interactively fit bi-Maxwellians for multiple (selectable) species to the reduced velocity distributions. The advantage of such software is that it can account for situations with multiple proton beams in addition to the alpha-particle population and even O^{6+}. The software will be completed and released for public use within the time range of this proposal.

All of the FC data products are archived at the SPDF active archive. The FC data products are summarized in the SWE Ion Table.

SWE Electrons

Documentation: The SWE electron sub-system consists of two electrostatic analyzers, the vector spectrometer (VEIS) and the Strahl spectrometer. They were designed to measure the solar wind electron distribution function. The sensors are fully described by *Ogilvie et al.* [1995] and the instrument description portion of this paper can also be found at the *Wind* project web page (http://wind.nasa.gov).

Due to a high voltage supply failure the last available data from the VEIS detector is May 31, 2001. Since the Strahl detector has very similar capabilities (though it was used in a different manner at the beginning of the mission) it was reprogrammed and the ground software rewritten to recover the electron moment and pitch angle measurements originally supplied by VEIS. The SWE Space Science Review article has been updated with these modifications and is available at the *Wind* project page along with a technical description of the new ground software algorithms. Moreover, the headers of the CDF data files have extensive documentation for each data product.

Data Products: There are four SWE electron data products: (1) electron moments containing electron density, velocity, temperature and heat flux parameters; (2) the pitch angle files providing electron fluxes at 30 directional bins relative to the instantaneous magnetic field direction at 13 different energy levels; (3) the averaged pitch angle data product with various aggregate averages formed from the complete pitch angle data; (4) and finally the strahl data with higher angular resolution electron pitch angle observations near the magnetic field direction. Starting on Aug 16, 2002, all of these four data products are generated by the new production software based on the reprogrammed Strahl detector measurements. In addition, the electron "moments" are no longer the result of integral moment calculations but estimated from the fitting of a single kappa distribution function to both the core and halo components. Except for the Strahl data, all electron data products are available through CDAWeb. The strahl data is available from the instrument web page. The current availability of the SWE electron data products is summarized in the table below.

SWE Electron Data	Cadence	Coverage	Format	Location
Moments (H0)	12 s	1994/12/29–2001/05/31	CDF	SWEFTP[a], CDAWeb[b]
Pitch-angle (H4)	12 s	1994/12/29–2001/05/31	CDF	SWEFTP, CDAWeb
Avg. Pitch-angle (M2)	12 s	1994/12/29–2001/05/31	CDF	SWEFTP, CDAWeb
Strahl	12 s	1994/12/29–2001/05/31	binary	SWEFTP
New Moments (H5)	12-15 s	2002/08/16–Present	CDF	SWEFTP, CDAWeb
New Pitch-angle (H3)	12-15 s	2002/08/16–Present	CDF	SWEFTP, CDAWeb
New Avg. Pitch-angle (M0)	12-15 s	2002/08/16–Present	CDF	SWEFTP, CDAWeb
New Strahl	12-15 s	2002/08/16–Present	CDF	SWEFTP

[a] ftp://windswe.gsfc.nasa.gov/pub; [b] http://cdaweb.gsfc.nasa.gov

3DP

Documentation: The *Wind*/3DP instrument consists of six different sensors. There are two electron (EESA) and two ion (PESA) electrostatic analyzers with different geometrical factors and fields-of-view. This way, they can cover the wide dynamic range from 3 eV to 30 keV that encompasses the bulk of the solar wind and much lower density suprathermal populations. There are also a pair of solid state telescopes (SST) the measure electrons with energies up to 400 keV and protons with energies up to 6 MeV. The instrument is fully described by *Lin et al.* [1995]. The instrument description portion of this paper is reproduced at the *Wind* project web site.

The PESA and EESA detectors are swept over their energy range typically 32 times per the 3-second spacecraft spin rate to produce very high time resolution 3D distributions. This process results in a very large volume of data that cannot all be telemetered to the ground. Thus, extensive use is made of onboard processing capabilities. As a result a large number of 3DP data products were developed, some based on onboard processing and some generated on the ground. Some documentation of these data products exist at the 3DP instrument web page (http://sprg.ssl.berkeley.edu/wind3dp/). Extensive 3DP metadata can also be publicly located on VHO.

Data Products: As most *Wind* instruments, 3DP team has provided a KP production software to be run automatically at the PWG system. This data product contains electron and ion fluxes at seven energies for each particle and some basic moment computations and can be found at CDAWeb for the whole duration of the mission. Much more popular is the unique 3 second time resolution onboard proton moment (PM) data. Even though it is computed onboard the spacecraft it has proven very reliable. It can be accessed for the complete mission at both the 3DP instrument site and at CDAWeb. In addition, the 24-second time resolution ion omni-directional fluxes and the 98-second electron omni-directional fluxes can also be obtained at both the 3DP and CDAWeb sites along with the electron piych angle distributions.

New *Wind*/3DP data sets wer made publicly available recently on CDAWeb. The new data includes: suprathermal electron pitch-angle and omni-directional energy spectra for $\sim$ 130 eV to $\sim$ 30 keV (EESA High or wi_eh*_3dp_* files) and for $\sim$ 20 keV to $\sim$ 500 keV (solid-state telescope, or SST, foil or wi_sf*_3dp_* files); suprathermal proton pitch-angle and omni-directional energy spectra for $\sim$ 70 keV to $\sim$ 7 MeV (SST Open or wi_so*_3dp_* files).

The current status of the 3DP data products is listed in the table below. All of them cover the full mission duration from 1994/11/15 to present.

3DP Data Product	Cadence	Coverage	Format	Location
KP	92 s	Entire Mission	CDF	CDAWeb[a]
PM[b]	3 s	Entire Mission	CDF	CDAWeb, Berkeley[c]
ELSP[d]	24-98 s	Entire Mission	CDF	CDAWeb, Berkeley
PLSP[d]	24 s	Entire Mission	CDF	CDAWeb, Berkeley
ELPD[d]	24-98 s	Entire Mission	CDF	CDAWeb, Berkeley
PLPD	24 s	Entire Mission	CDF	CDAWeb, Berkeley
SST[e] SFSP[f]	12 s	Entire Mission	CDF	CDAWeb, Berkeley
SST SOSP[f]	12 s	Entire Mission	CDF	CDAWeb, Berkeley
SST SFPD	12 s	Entire Mission	CDF	CDAWeb, Berkeley
SST SOPD	12 s	Entire Mission	CDF	CDAWeb, Berkeley

[a] http://cdaweb.gsfc.nasa.gov; [b] onboard proton moments; [c] http://sprg.ssl.berkeley.edu/wind3dp/;
[d] EL = electron; PL = proton; SP = omni directional fluxes; PD = pitch-angle; [e] SST = solid state telescope;
[f] SF = foil (electrons); SO = open (protons)

SMS

Documentation: The *Wind* SMS instrument suite is composed of three separate instruments. The SupraThermal Ion Composition Spectrometer (STICS) determines mass, mass per charge, and energy for ions in the energy range from 6-230 keV/e. The high resolution mass spectrometer (MASS) determines elemental and isotopic abundances from $\sim$0.5-12 keV/e. Finally, the Solar *Wind* Ion Composition Spectrometer (SWICS) experienced a failure of the "stop" MCP and hence has reduced capabilities. Initially, it provided mass, charge, and energy for ions in the energy range of $\sim$0.5-30 keV/e. However, since the failure the particles mass and charge cannot be uniquely determined and no data is currently processed from it. These instruments are fully described by

SMS Data Product	Cadence	Coverage	Format	Location
KP SWICS+STICS	4 hr	1994/12/12–2000/05/27	CDF	CDAWeb[a]
STICS[b]	1 day	1995/01/01–2007/12/31	ASCII	*Wind* Project[c]
SWICS+MASS[d]	1 hr	Select Days	ASCII	UMichigan[e]

[a] http://cdaweb.gsfc.nasa.gov; [b] proton and alpha-particle distribution functions; [c] http://wind.nasa.gov; [d] energy spectra; [e] http://pooh.engin.umich.edu/data.php

Gloeckler et al. [1995]. The Instrument calibration is fully described by *Ghielmetti et al.* [1983] and in the PhD thesis of K. Chotoo both available at the *Wind* project page. Additional data release notes are archived at the VHO.

Data Products: Till the failure of the SWICS instrument (May 27, 2000), combined SWICS and STICS KP files were generated that contain alpha particle information along with some carbon and oxygen abundances and temperatures. This data product is still publicly available from CDAWeb. Since the SWICS failure, a lot of time went into determining how to properly use the other two sensors by themselves. A new software system has been developed which automates many data analysis functions previously done manually. This system first simultaneously assigns events to specific ion species, removing any overlap and using the statistical properties of the measurements to maximum advantage. It then uses these assigned events to construct phase space density distribution functions and corrects these for the effects of instrument efficiency and sampling geometry. Finally, it outputs these distribution functions, error estimates, and count rates for each ion along with many intermediate products that facilitate detailed analysis. The software can perform arbitrary time integrations of the data and can optionally use an inversion method to remove overlap among ions in the instrument measurement space. Development of this system is in the data validation and optimization stage, with the first scientific analyses already underway.

Daily averages of the proton and alpha particle phase space density distribution functions for the whole mission is already publicly available through the *Wind* project web page. In addition, hourly resolution STICS and MASS energy spectra for select days by request throughout the mission are available in digital and graphical formats from the University of Michigan page (http://pooh.engin.umich.edu/data.php) and . Further work is under way to produce more data products. The current status of the SMS data products is summarized in the table shown above.

EPACT

Documentation: The Energetic Particles: Acceleration, Composition and Transport (EPACT) investigation consists of multiple telescopes. The highest energy telescopes (APE and IT) have failed early in the mission. However, the Low Energy Matrix Telescope (LEMT) covering energies in the 1-10 MeV/nuc range and the Suprathermal Energetic Particle telescope (STEP) measuring ions heavier than protons in the 20 keV to ∼1 MeV/nuc range still continue to provide valuable data. These instruments have been described by *von Rosenvinge et al.* [1995]. The instrument portion of this paper is reproduced at the *Wind* project web page (http://wind.nasa.gov). Additional instrument information is available at the instrument web page (http://epact2.gsfc.nasa.gov/). The newly generated sectored count data is described also at the *Wind* project web page.

Data Products: Fluxes for a select number of ions (helium, oxygen, iron and combined CNO) in energy bins below 1 Mev/nuc and averaged over 92 seconds are publicly available for the whole mission in KP files at CDAWeb. As a quick look at this data reveals, the count rate of these energetic particles is very low, thus most of the KP data points are identically zero. In past, select time periods with intense particle events were manually analyzed and higher level data products generated from them. These were available on request to the public. More recently, a systematic search for events with non-zero count rates have been undertaken, and 41 such several day long periods identified in the 1997-2006 time range. For these intervals hourly resolution ion sectored count data (SEC) were generated. This is a unique *Wind* data product of the directional distribution of energetic particles in teh ecliptic. These ASCII text files are publicly available at the *Wind* project web page. In addition, the first order ion anisotropy from these observations was computed. These results are also available from the *Wind* project web page. This effort will continue and more event files will be made public once the Sun becomes more active again. The current status of the EPACT data sets is summarized in the table below.

Hourly-averaged omnidirectional particles fluxes from LEMT subsystem of the *Wind*/EPACT instrument are available from OMNIWeb and SPDF. The data cover the entire mission from 3 November 1994 – 6 September 2014 and will be updated periodically. The data include He, C, O, Ne, Si, and Fe in seven energy bins (six for

EPACT Data Product	Cadence	Coverage	Format	Location
KP fluxes	92 s	1994/11/16–Present	CDF	CDAWeb[a]
OMN[b]	1 hr	1994/11/03-2014/09/06	ASCII	OMNIWeb[c]
SEC[d]	1 hr	41 Events	ASCII	*Wind* Project[e]
Anisotropy	1 hr	39 Events	ASCII	*Wind* Project

[a] http://cdaweb.gsfc.nasa.gov; [b] omnidirectional fluxes; [c] http://omniweb.gsfc.nasa.gov; [d] http://wind.nasa.gov; [e] sectored counts

Ne) from ∼2–10 MeV/nucleon. The OMNIWeb Plus browser can be used to generate time–intensity profiles and correlation plots. In addition, the Multi–Source Spectra Plot Interface of the OMNIWeb-related Virtual Energetic Particle Observatory (VEPO) allows easy comparison of LEMT ion spectra with simultaneous measurements from ACE (ULEIS, EPAM, and SIS) and the STEREO (SIT and LET). Locations of the LEMT data can be found in the Heliophysics Data Portal using the text restriction "LEMT". The highest time resolution, 5-minute data is is currently prepared for public release.

MFI

Documentation: The *Wind* Magnetic Field Investigation (MFI) is composed of two fluxgate magnetometers located at the mid point and end of a long boom. The instrument measures DC vector magnetic fields up to a time resolution of ∼22 or ∼11 vectors/sec depending on the telemetry mode of the spacecraft. The instrument is completely described in an article by *Lepping et al.* [1995]. The instrument description sections of this paper are reproduced at the *Wind* project web page (http://wind.nasa.gov).

The data processing algorithms employed in generating the MFI data products are described by *Farrell et al.* [1995]. This paper is also available at the *Wind* Project web page. The largest source of uncertainty in the MFI data is the inherent rms noise due to averaging. The vector rms noise is computed for all data points and for all time averages from the raw telemetered resolution data and is included in the distributed data files.

Data Products: The MFI team essentially generates only one kind of data product, the vector magnetic fields, at various time resolutions and with increasing quality of calibrations. Within 24 hours of measurement, the 92-second KP data is publicly available at CDAWeb. This data uses periodically updated calibration tables. Typically, with no longer than 2 week delay, the MFI team produces a calibrated data product that includes 3-second, 1 minute and 1 hour averages. This data product (version 3) has the final calibrations in the spacecraft spin plane and preliminary calibration along the spin axes. Requiring at least of 1 month of time lag, the final spin axis corrections can be computed with uncertainties of no more than a few tenths of a nT. These files (version 4) are also uploaded to CDAWeb where they replace the version 3 files. Finally, after 2-3 months, all spacecraft noise effects can be included and final, archival quality data (version 5) is generated and uploaded to CDAWeb. All of these versions have the exact same internal format. To encourage the use of the higher quality data products, CDAWeb keeps only the latest year of KP data on-line. All MFI data is backed up in the SPDF final active archive.

Till recently, the full ∼11 or ∼22 vectors/sec data was too large in volume to serve on-line and has been stored on tapes and made publicly available on request. Recently, after significant effort, the artificial spin tones were successfully reduced in this high time resolution data and was packaged in CDF format and distributed through CDAWeb and VHO.

The current status of the MFI data products is summarized in the table below.

MFI Data Product	Cadence	Coverage	Format	Location
KP	92 s	2010/09/01–Present	CDF	CDAWeb[a]
Versions 3 & 4	3 s, 1 min, 1 hr	1994/11/16–Present	CDF	CDAWeb
Version 5	3 s, 1 min, 1 hr	1994/11/16–Present	CDF	CDAWeb
High Res.	∼11 or ∼22 vec/sec	1994/11/16–Present	CDF	CDAWeb

[a] http://cdaweb.gsfc.nasa.gov

WAVES

Documentation: The *Wind* WAVES experiment composed of the RAD1, RAD2 and TNR receivers measures electric fields in a wide range of frequencies. The instrument is fully documented by *Bougeret et al.* [1995]. The instrument related sections of this paper are reproduced at the *Wind* project web page (http://wind.nasa.gov). Some additional documentation exists also at the WAVES instrument web page

(http://www-lep.gsfc.nasa.gov/waves/). The content and format of the various WAVES data products are also described on the instrument web page.

Data Products: As most other *Wind* instruments, WAVES also produces a KP data product that is immediately publicly available at CDAWeb. The WAVES KP data contains 3-minute averages of the electric field intensities at 76 log-spaced frequencies and electron density estimates based on neural network determined electron plasma frequency values. In addition, the team produces, with no more than 1 week delay, higher time resolution (1 minute) normalized receiver voltages and makes it available both at CDAWeb and on their own web site. This is the fundamental data product that is used for the generation of the familiar WAVES frequency vs. time intensity plots. These plots are also pre-generated and publicly available on the instrument web page in PDF format. Finally, 7-10 second time resolution electron density estimates are also computed and made available at CDAWeb.

The WAVES team also maintains a Type II/IV catalog on their web site that is widely used. The current status of the WAVES data products is summarized in the table below.

Software Tools: Unlike the other *Wind* instrument teams, the WAVES team distributes primarily the lowest level data they have without generating many higher level products. Therefore, dedicated software tools are necessary for non-specialists to make use of this data. The team maintains a small IDL software library on their web site that readily ingests the downloaded IDL save files and allows the custom generation of data plots.

Future Data Products: The WAVES instrument also returns short waveform captures from the time domain sampler (TDS) receiver of high frequency electric and magnetic field observations in two and three dimensions. The team is currently finalizing software that will produce all the TDS events for the entire mission to be put on CDAWeb. The data product will include all the relevant information that went into processing the final results. Each TDS event is composed of multiple channels (2 or 4, depending on the operating mode) containing either two electric field components in fast mode (TDSF) or three magnetic(electric) and one electric(magnetic) field components in slow mode (TDSS). The data is sampled at commandable rates between ∼117 sps and ∼120,000 sps, corresponding to ∼0.017–17.5 second duration waveform captures. The data products will be provided in CDF format and released for public use on CDAWeb.

David Malaspina (PI) and Lynn. B. Wilson III (Co-I) were funded from an HGI-ODDE ROSES proposal to produce a dust impact database for the entire *Wind* mission using the TDSF events. The dust impact database will consist of CDF files containing information on each identified dust impact, including the date and time, orientation of the spacecraft, and impact location on the spacecraft body. The completed data set will be archived and made publicly available through NASAs Space Physics Data Facility (SPDF) at CDAWeb.

WAVES Data Product	Cadence	Coverage	Format	Location
KP	3 min	1994/11/10–Present	CDF	CDAWeb[a]
TNR[b], Rad1, Rad2[c]	1 min	1994/11/10–Present	ASCII, IDL Save	CDAWeb, WAVES[d]
High Res. n_e[e]	7-10 s	1994/11/10–Present	CDF	CDAWeb
Radio Plots	1 min	1994/11/10–Present	PNG, PDF	WAVES

[a] http://cdaweb.gsfc.nasa.gov; [b] Thermal Noise Receiver; [c] Radio Receiver Band 1, 2;
[d] http://www-lep.gsfc.nasa.gov/waves/; [e] electron number density;

KONUS and TGRS

The KONUS and TGRS γ-ray instruments are not maintained by heliophysics. Their data production and data distribution is completely handled by the astrophysics division. Description of the instruments and links to their data products can be found at (http://heasarc.gsfc.nasa.gov/docs/heasarc/missions/wind.html).

Wind and VHO

Members of the *Wind* instrument teams have taken leadership roles in the development of the Virtual Heliospheric Observatory (VHO) (http://vho.nasa.gov). Aside from assuring that the various data products are publicly open, the most effort went into the generation of SPASE dictionary based and VHO compliant metadata. In fact, the first *Wind* data product metadata files have been used to refine the SPASE dictionary for fields and particles data. Currently, all primary *Wind* data products are fully searchable via the VHO.

Acronyms and Initialisms

3D . . . . . three-dimensional

3DP . . . . . Three-Dimensional Plasma and Energetic Particle Investigation (*Wind*/3DP)

ACE . . . . . Advanced Composition Explorer

ACR . . . . . Anomalous Cosmic Ray

APE . . . . . Alpha-Proton-Electron telescope (part of *Wind* EPACT/ELITE)

ARTEMIS . . . . . Acceleration, Reconnection, Turbulence and Electrodynamics of the Moon's Interaction with the Sun

AU . . . . . Astronomical Unit

CAP . . . . . Command and Attitude Processor

CCMC . . . . . Coordinated Community Modeling Center

CIR . . . . . Corotating Interaction Region

CME . . . . . Coronal Mass Ejection

DSA . . . . . Diffusive Shock Acceleration

DSCOVR . . . . . Deep Space Climate Observatory

DSN . . . . . Deep Space Network

E/PO . . . . . Education and Public Outreach

EESA . . . . . Electron Electrostatic Analyzer (*Wind*/3DP)

EH . . . . . Electron Hole

ELITE . . . . . Electron-Isotope Telescope system (*Wind*/EPACT)

EPACT . . . . . Energetic Particles: Acceleration, Composition, and Transport (APE-ELITE-IT-LEMT package on *Wind*)

ESA (agency) . . . . . European Space Agency

ESW . . . . . Electrostatic Solitary Wave

FAB . . . . . Field-Aligned (ion) Beam

FC . . . . . Faraday Cup

FOT . . . . . Flight Operations Team

FTE . . . . . Full Time Equivalent

GCN . . . . . Gamma-ray Coordinates Network

GeV . . . . . Giga-electron volt

GF . . . . . Giant Flares

GGS . . . . . Global Geospace Science

GLE . . . . . Ground-Level Events

GOES . . . . . Geostationary Operational Environmental Satellites

GRBs . . . . . Gamma Ray Bursts

GSFC . . . . . Goddard Space Flight Center

HETE-2 . . . . . High Energy Transient Explorer-2

HGO . . . . . Heliophysics Great Observatory

HI . . . . . Heliospheric Imagers

HSO . . . . . Heliophysics System Observatory

HTR . . . . . High Time Resolution

IBEX . . . . . Interstellar Boundary Explorer

ICME . . . . . Interplanetary Coronal Mass Ejection

IMAP . . . . . Interstellar MApping Probe

IMF . . . . . Interplanetary Magnetic Field

IMPACT . . . . . In-situ Measurements of Particles and CME Transients (suite)

IP . . . . . Interplanetary

IPD . . . . . Interplanetary Dust

IPM . . . . . Interplanetary Medium

IPN . . . . . Interplanetary GRB Network

ISD . . . . . Interstellar Dust

ISS . . . . . International Space Station

ISTP . . . . . International Solar-Terrestrial Physics

IT (detector) . . . . . Isotope Telescope (part of *Wind* EPACT/ELITE)

ITOS . . . . . Integrated Test and Operations System

keV . . . . . kilo-electron volt

KH . . . . . Kelvin-Helmholtz

KONUS . . . . . Gamma-Ray Spectrometer

KP . . . . . Key Parameter

LASCO . . . . . Large Angle and Spectrometric COronagraph

LEMT . . . . . Low Energy Matrix Telescopes (*Wind*/EPACT)

LET . . . . . Low Energy Telescope

LWS . . . . . Living With a Star

LZ . . . . . Level Zero

MASS . . . . . high-resolution mass spectrometer (*Wind*/SMS)

MAVEN . . . . . Mars Atmosphere and Volatile EvolutioN mission

MC . . . . . Magnetic Cloud

MESSENGER . . . . . Mercury Surface Space Environment Geochemistry and Ranging

MeV . . . . . Mega-electron volt

MHD . . . . . Magnetohydrodynamic

MMOC . . . . . Multi-Mission Operations Center

MMS . . . . . Magnetospheric Multi-Scale NASA STP mission

MOVE . . . . . Mission Operations Voice Enhancement

NASA . . . . . National Aeronautics and Space Administration

PESA . . . . . Ion Electrostatic Analyzer (*Wind*/3DP)

PMS . . . . . Planar Magnetic Structure

PWG . . . . . Polar-Wind-Geotail ground system

RBSP . . . . . Radiation Belt Storm Probes (now *Van Allen Probes*)

RHESSI . . . . . Reuven Ramaty High Energy Solar Spectroscopic Imager

SDO . . . . . Solar Dynamics Observatory

SECCHI . . . . . Sun-Earth Connection Coronal and Heliospheric Investigation

SEP . . . . . Solar Energetic Particle

SEU . . . . . Single Event Upset

SGR . . . . . Soft Gamma Repeaters

SHH . . . . . soft-to-hard-to-harder (i.e., change for X-ray spectra)

SIR . . . . . Stream Interaction Region

SIS . . . . . Solar Isotope Spectrometer

SLAMS . . . . . Short Large Amplitude Magnetic Structures

SMD . . . . . Science Mission Directorate

SMS . . . . . Solar Wind and Suprathermal Ion Composition Experiment (SWICS-MASS-STICS package on *Wind*)

SOHO . . . . . SOlar and Heliospheric Observatory

SolO . . . . . Solar Orbiter mission

SPASE . . . . . Space Physics Archive Search and Extract

SPP . . . . . Solar Probe Plus mission

sps . . . . . samples per second

SSMO . . . . . Space Science Mission Operations

SSN . . . . . Sun Spot Number

SST . . . . . Solid-State (semi-conductor detector) Telescope (*Wind*/3DP)

STEP . . . . . SupraThermal Energetic Particle Telescope (*Wind*/EPACT)

STEREO . . . . . Solar-Terrestrial Relations Observatory

STICS . . . . . SupraThermal Ion Composition Spectrometer (*Wind*/SMS)

SWE . . . . . Solar Wind Experiment

SWEPAM . . . . . Solar Wind Electron Proton Alpha Monitor (ACE)

SWICS . . . . . Solar Wind Ion Composition Spectrometer (*Wind*/SMS)

TD . . . . . Tangential Discontinuity

TDS . . . . . Time Domain Sampler (*Wind*/WAVES)

TDSF . . . . . Time Domain Sampler Fast (*Wind*/WAVES)

TDSS . . . . . Time Domain Sampler Slow (*Wind*/WAVES)

TGRS . . . . . Transient Gamma-Ray Spectrometer

THEMIS . . . . . Time History of Events and Macroscale Interactions during Substorms

TNR . . . . . Thermal Noise Receiver (e.g., part of *Wind*/WAVES)

TPOCC . . . . . Transportable Payload Operations Control Center

TRACE . . . . . Transition Region And Coronal Explorer

ULEIS . . . . . Ultra Low Energy Isotope Spectrometer

VDS . . . . . Voice/Video Distribution System

VEIS . . . . . Vector Ion-Electron Spectrometers (*Wind*/SWE)

VEX . . . . . Venus EXpress

VHO . . . . . Virtual Heliophysics Observatory

VWO . . . . . Virtual Waves Observatory

WYE . . . . . Work Year Equivalent